E&G Quaternary Sci. J., 73, 1–22, 2024
https://doi.org/10.5194/egqsj-73-1-2024

Open Access E&G Quaternary Science Journal

Research article

Reconstructing the Eemian to Middle Pleniglacial pedosedimentary evolution of the Baix loess–palaeosol sequence (Rhône Rift Valley, southern France) – basic chronostratigraphic framework and palaeosol characterisation

Nora Pfaffner[1,2], Annette Kadereit[3], Volker Karius[4], Thomas Kolb[5], Sebastian Kreutzer[3,6,7], and Daniela Sauer[1]

[1]Department of Physical Geography, University of Göttingen, 37077 Göttingen, Germany
[2]Institute of Forest Ecosystems, Thünen Institute, 16225 Eberswalde, Germany
[3]Heidelberg Luminescence Laboratory, Institute of Geography, University of Heidelberg, 69120 Heidelberg, Germany
[4]Department of Sedimentology and Environmental Geology, University of Göttingen, 37077 Göttingen, Germany
[5]Department of Geography, University of Giessen, 35390 Giessen, Germany
[6]Geography & Earth Sciences, Aberystwyth University, Aberystwyth, SY23 3DB, Wales, United Kingdom
[7]Archéosciences Bordeaux, UMR 6034, CNRS – Université Bordeaux Montaigne, 33607 Pessac, France

Correspondence: Nora Pfaffner (nora.pfaffner@protonmail.com)

Relevant dates: Received: 7 December 2022 – Revised: 9 July 2023 – Accepted: 25 October 2023 – Published: 9 January 2024

How to cite: Pfaffner, N., Kadereit, A., Karius, V., Kolb, T., Kreutzer, S., and Sauer, D.: Reconstructing the Eemian to Middle Pleniglacial pedosedimentary evolution of the Baix loess–palaeosol sequence (Rhône Rift Valley, southern France) – basic chronostratigraphic framework and palaeosol characterisation, E&G Quaternary Sci. J., 73, 1–22, https://doi.org/10.5194/egqsj-73-1-2024, 2024.

Abstract: Loess–palaeosol sequences (LPSs) are important archives of landscape evolution, recording alternating periods of geomorphic activity (dust deposition and slope processes) and landscape stability (soil formation). LPSs of the Rhône Rift Valley are located along a spatial climatic gradient from the mid-latitudes to the Mediterranean region. This position renders them extremely valuable archives for correlating LPSs in the European loess belt and the Mediterranean region. Despite this important function, Rhône Rift Valley LPSs have been little investigated. In this study, we aimed to narrow this knowledge gap, in a first step towards linking LPS-based mid-latitude and Mediterranean palaeoenvironmental reconstructions. We studied the ∼ 14 m thick Baix LPS located at the western edge of the Rhône Rift Valley near Valence. Here, we focus on the lower ∼ 7 m of the LPS, which comprises 12 of 19 soil horizons overall, and record regional palaeoenvironmental variations from the Eemian to the Middle Pleniglacial (∼ marine isotope stage (MIS) 5 to MIS 3). Our reconstruction is based on detailed field description, complemented by granulometry (10 cm vertical resolution), and micromorphological analyses. Luminescence screening of cut-out soil-sediment columns subsampled with ∼ 5 cm vertical resolution (126 subsamples over 7 m) provides a preliminary chronometry. The loess deposits of the Baix LPS are strongly calcareous and predominantly silty but also contain sandy and fine gravelly laminae typical of loess deposits subjected to slope-wash processes. From bottom to top, the investigated part shows three intensely pedogenised levels: (1) a basal sequence of reddish-brown Btg and Bt horizons of a thick Eemian Stagnic Luvisol (MIS 5e); (2) an early glacial yellowish-brown

Bw horizon (MIS 5d-a); and (3) a yellowish-brown Bw horizon with large cone-shaped carbonate nodules in the associated underlying Bk horizon, interpreted as a truncated Middle Pleniglacial (MIS 3) Calcic Cambisol. The Baix LPS is in parts very similar to the Collias LPS ∼ 100 km further south but also exhibits differences, reflecting its position at the spatial climatic transition between the presently temperate and the Mediterranean zone.

Kurzfassung:

Löss-Paläoboden-Sequenzen (LPS) stellen wichtige Archive der Landschaftsentwicklung dar. Sie dokumentieren den Wechsel zwischen geomorphologisch aktiven Phasen (mit Staubablagerung und Hangprozessen) und Phasen der Landschaftsstabilität (Bodenbildung). Die LPS entlang des Rhône-Grabens liegen innerhalb des Gradienten von derzeit gemäßigtem zu mediterranem Klima. Sie sind daher potentiell sehr wertvolle Archive, um die gut untersuchten LPS des Europäischen Lössgürtels und des Mediterranraums zu verknüpfen. Trotz dieser wichtigen Funktion wurden LPS des Rhône-Grabens bisher kaum untersucht, so dass diesbezüglich eine entsprechende Forschungslücke besteht. Mit dieser Arbeit stellen wir die ∼ 14 m mächtige Baix LPS am westlichen Rand des Rhône-Grabens bei Valence vor. Unser Fokus liegt auf den unteren ∼ 7 m der LPS, die 12 von insgesamt 19 identifizierten Bodenhorizonten enthalten und in denen regionale Änderungen der Paläoumwelt vom Eem bis zum Mittleren Pleniglazial (marine Isotopenstadien (MIS) 5 bis MIS 3) aufgezeichnet und archiviert wurden. Eine detaillierte Profilbeschreibung wird durch granulometrische Daten (10 cm Probenauflösung), mikromorphologische Untersuchungen und ein Lumineszenz-Screening an äquidistant, alle 5 cm genommenen Proben (126 Proben entlang der 7 m) ergänzt. Durch das Lumineszenz-Screening wird eine vorläufige Chronometrie erstellt. Die Lössablagerungen sind stark kalkhaltig und dominant schluffig, enthalten aber auch sandigere Lagen, die eine sekundäre Umlagerung anzeigen. Vom Liegenden zum Hangenden zeigt der untersuchte Abschnitt drei paläopedologisch intensiv überprägte Bereiche: (1) eine basale Abfolge rötlicher Btg- und Bt-Horizonte eines eemzeitlichen Stagnic Luvisols; (2) einen frühglazialen braunen Bw-Horizont (MIS 5a-d); und (3) einen braunen Bw-Horizont mit großen, zapfenförmigen Karbonatkonkretionen im unterliegenden Bk-Horizont, wobei Bw und Bk als Relikt eines teilweise erodierten, mittelpleniglazialen (MIS 3) Cambisols interpretiert werden. Die Baix LPS ist der Collias LPS ∼ 100 km weiter südlich teilweise sehr ähnlich, weist aber auch Unterschiede auf, die ihre Lage am räumlichen klimatischen Übergang zwischen der aktuell gemäßigten und der mediterranen Zone widerspiegeln.

1 Introduction

Loess–palaeosol sequences (LPSs) are valuable palaeoenvironmental archives, as they preserve information on, for example, past phases of (i) deposition of dust eroded from bare hillslopes and dried-out riverbeds and (ii) soil development and vegetation cover (e.g. Moine et al., 2005; Marković et al., 2009; Zech et al., 2012). In Europe, LPSs of large river basins have been intensively investigated in the mid-latitude region, e.g. in the Seine, Somme and Rhine basins (Bibus and Semmel, 1977; Guenther, 1987; Antoine et al., 2001, 2009, 2016, 2021; Schirmer, 2002, 2016; Fischer et al., 2021) as well as in the Mediterranean region, e.g. in the Ebro, Tagus and Po basins (Ferraro, 2009; Wacha et al., 2011; Boixadera et al., 2015; Zerboni et al., 2015; Costantini et al., 2018; Wolf et al., 2019). Yet, LPSs in the transition between the European mid-latitudes and the Mediterranean zone have remained rarely investigated. A few exceptions are early studies from the first half of the 20th century (Suen, 1934; Mazenot, 1956; Bonifay, 1965), when modern techniques of LPS analysis were not yet available.

The Rhône Rift Valley in SE France is a natural N–S-orientated corridor leading from the mid-latitudes to the Mediterranean zone. The area around 45° N (near Valence, Fig. 1) denotes the present-day transition between temperate and Mediterranean climate (Joly et al., 2010). Loess along the Rhône Rift Valley was intensively studied in the middle of the last century (Suen, 1934; Mazenot, 1956; Bourdier, 1958; Bonifay, 1965), when major construction works facilitated access to thick profiles. Source areas of the loess were the dried-out riverbeds of the Rhône River and its tributaries from the Alps and the Massif Central, which during glacial periods were fed with fine-grained material abraded by the glaciers in the western Alps and the Massif Central (Bosq et al., 2020a). Only recently has loess research in the area been resumed, applying state-of-the-art investigation methods, including numerical dating (Franc et al., 2017; Bosq et al., 2018, 2020a, b; Kreutzer et al., 2021; Mologni et al., 2021). One of the recently reinvestigated LPSs is the Collias LPS, located in the Mediterranean zone of SE France (Fig. 1). There, a prominent Middle Pleniglacial (marine iso-

tope stage (MIS) 3) yellowish-brown palaeosol horizon was observed. Optically stimulated luminescence (OSL) dating (e.g. Aitken, 1998) suggested a time window for the formation of this palaeosol of between ∼ 55 ± 4 ka (deposition of the sediment the palaeosol had developed in) and ∼ 39±3 ka (sediment accumulation on top of the palaeosol) (Bosq et al., 2020b). The underlying soil horizon exhibited large cone-shaped carbonate nodules, resulting from substantial carbonate leaching from the Middle Pleniglacial palaeosol horizon and associated carbonate reprecipitation below. We observed these characteristic carbonate nodules in several LPSs along the Rhône Rift Valley.

At the base of the Collias LPS, several reddish-brown palaeosol horizons with stagnic properties were observed and interpreted as the MIS 5 palaeosol complex. They were underlain by a massive calcrete (Bosq et al., 2020b). The ∼ 14 m thick Baix LPS is situated at 44°42.5′ N, thus within the transition from presently temperate to Mediterranean climate, which makes it a promising candidate for linking the European mid-latitude and Mediterranean LPSs.

Therefore, the aim of the present study was to assess the potential of the Baix LPS for landscape reconstruction. Based on the similarity with the Collias LPS (∼ 100 km further south), we assumed that the Baix LPS encompasses the same time span, i.e. the last interglacial and last glacial period. Here, we focus on the lower ∼ 7 m of the Baix LPS, reaching from a basal reddish-brown palaeosol horizon sequence (12.0–13.7 m depth) up to a yellowish-brown palaeosol horizon sequence with large carbonate nodules at its base (735–853 cm depth), very similar to the Middle Pleniglacial palaeosol in the Collias LPS. Our approach includes a detailed field description, complemented by granulometric analysis (10 cm vertical resolution) and micromorphological observations together with an approximate chronometric framework. The preliminary age assessment is based on OSL screening on minimally prepared material (∼ 1 cm^3 samples), collected at ∼ 5 cm spatial resolution. Reconstructed phases of geomorphic and pedogenic evolution at the Baix LPS were compared to other regional palaeoenvironmental archives (Fig. 1). These include pollen records from lacustrine and marine sediments (Les Échets, Velay, Gulf of Lion), considering their variations in latitude and altitude (Beaulieu and Reille, 1984a, b, 1989; Reille and Beaulieu, 1990; Reille et al., 2000; Guiter et al., 2003; Beaudouin et al., 2005), as well as sediment records from archaeological cave and/or rock-shelter sites.

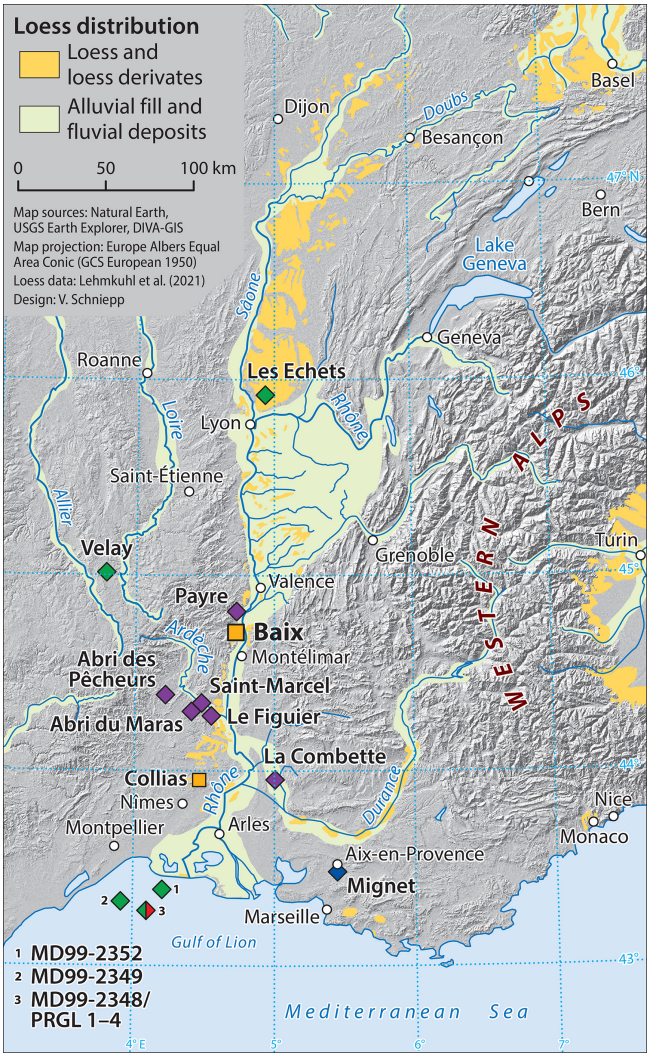

Figure 1. Location of the Baix loess–palaeosol sequence (LPS) at the western edge of the Rhône Rift Valley and published archives used for comparison and complementation of the palaeoenvironmental reconstruction. The Baix and Collias LPSs are marked by orange squares. Pollen records (green diamonds) from lacustrine sediments of Les Échets (Beaulieu and Reille, 1984a, b); maar lakes in the Velay region, Lac du Bouchet, Ribains and Praclaux (Reille and Beaulieu, 1990; Reille et al., 2000); and marine sediments from the Gulf of Lion (cores: MD 99-2349, MD99-2352, MD99-2348/PRGL1-4; Beaudouin et al., 2005). Archaeological sites (purple diamonds) of Payre (Valladas et al., 2008; Rivals et al., 2009), La Combette (Kreutzer et al., 2021; Mologni et al., 2021), and the Ardèche area (Abri des Pêcheurs, Saint-Marcel, Le Figuier, Abri du Maras) (Moncel et al., 2015). Molluscan record (blue diamond) of Aix-en-Provence (Magnin and Bonnet, 2014). Marine sediment record (half-red diamond) from the Gulf of Lion (core/borehole PRGL1-MD99-2348; Sierro et al., 2009).

2 Study site, sampling and methods

2.1 Study site

The Baix LPS (44°42′36.30″ N, 4°43′20.80″ E) is located at the western edge of the Rhône Rift Valley, SW of Valence and ca. 4 km west of the Rhône River at an elevation of 155 m a.s.l. (Figs. 1, 2). It is situated on the foot slope of a

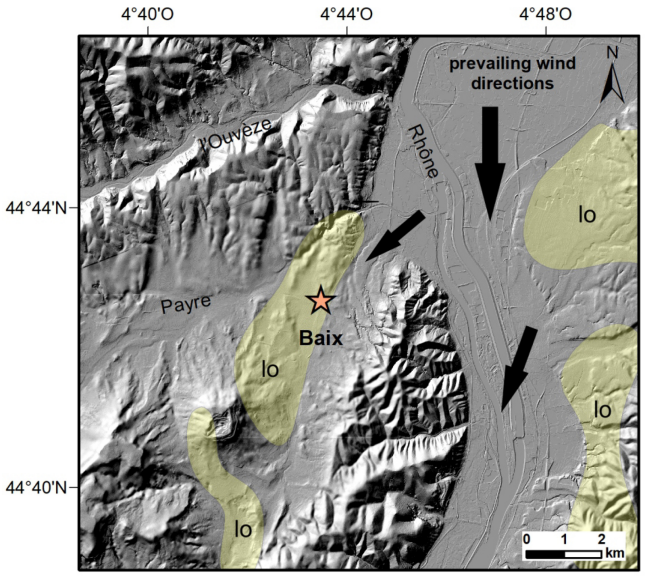

Figure 2. Hillshade map of the area around the Baix LPS, Rhône Rift Valley, SE France, with prevailing wind directions and distribution of loess and loess derivates (lo) derived from Lehmkuhl et al. (2021) (map data: DEM with a 5 m × 5 m resolution derived from IGN-FR, 2020).

convex ridge that forms the northern edge of a small basin, consisting of Lower Cretaceous limestone and marl, covered by Cretaceous debris and Pleistocene sediments (Chenevoy et al., 1977; Saint Martin, 2009).

To the south, the basin is bordered by the basaltic plateau of the Coiron volcanic province with the Montagne d'Andance (530 m a.s.l.), a volcano that was active until the Late Miocene to Pliocene times (Chenevoy et al., 1977; Pastre et al., 2004). Several episodic creeks drain the basin via the rivers Ouvèze and Payre in an eastern direction towards the Rhône River (Fig. 2). The present climate is characterised by a mean annual temperature of 13.3 °C and mean annual precipitation of 874 mm, with a precipitation maximum in October or November (Meteo-France, 2021). The predominant wind regime is the mistral, a strong northerly wind that is channelled within the Rhône Rift Valley and accelerated southward (Guenard et al., 2005). At the opening of the western shoulder of the Rhône Rift Valley near Baix, a part of the wind flow gets diverted westward into the small basin on whose northern edge the Baix LPS is located (Fig. 2). The Baix LPS is situated in the wind shadow with respect to the wind that blows from the Rhône Rift Valley into the basin immediately south of the low crest on whose foot slope the Baix LPS is located. This situation explains the occurrence of the thick loess patch at this south-facing foot slope.

The Baix LPS was first mentioned by Suen (1934) and named "Baix" by Mazenot (1956). Solely based on field observations, Mazenot (1956) subdivided the Baix LPS into four parts, comprising (1) a palaeosol at the base, containing debris of basalt and Cretaceous limestone, overlain by (2) decarbonated red loamy loess, superimposed by (3) typical yellow loess, and (4) typical loess on top. Mazenot (1956) interpreted the entire Baix LPS as having developed in one single loess deposit, arguing that the intensive alteration of the basal part occurred due to a high groundwater table in former periods.

2.2 Field description and sampling

2.2.1 Field description, palaeosol classification, sampling for granulometry and analyses of carbonate content and micromorphology

We cleaned a main vertical profile of 13.7 m on the eastern wall of a small loam pit during three field campaigns in the years 2018–2020 (Fig. 3a–e) and described it according to the *Guidelines for soil description* (FAO, 2006). Palaeosols were later classified according to the World Reference Base for Soil Resources (IUSS Working Group WRB, 2022). Sampling for granulometric analysis was done by taking mixed samples integrating over 10 cm, thus continuously sampling the whole section at 10 cm vertical resolution. Where a horizon boundary (characterised by distinct changes in texture, structure and/or colour) occurred in less than 10 cm distance, the sampling interval was adjusted to the horizon boundary. The samples were air-dried, sieved (< 2 mm mesh size) and homogenised. The coarse material (≥ 2 mm) was treated with 10 % HCl to dissolve possibly included carbonate nodules. It was then weighed to determine the rock-fragment content of the sediment as an important indicator of loess reworking through slope-wash processes. Three undisturbed, orientated blocks were collected from the main palaeosol horizons (5 Bw2, 7 Bt1) and unweathered loess (5 Ck2) for micromorphological analysis. These samples were taken in Kubiëna boxes (6 cm × 8 cm × 4 cm) that were gently inserted into the profile wall, steadily supported by a knife.

2.2.2 Sampling for luminescence screening

Material for luminescence screening was sampled semi-continuously from the lower ∼ 7 m of the previously cleaned profile wall. For this purpose, we carved into the profile wall to separate the sediment columns to be sampled (12 cm width; Fig. 3e). Then, we placed a plastic flower box vertically onto the uppermost section of the uppermost sediment column, with its opening towards the wall. We obtained a sediment block of ca. 43 cm × 12 cm × 10 cm by carving around the side walls of the flower box with long knives and saws. We repeated this procedure from the top to bottom of the sediment columns, obtaining one flower pot filled with a sediment block after the other. An unsampled space of 3 cm remained between two consecutive sediment blocks due to the protruding rims of the flower boxes. Irregularities in the profile wall that might affect the luminescence signal were avoided by sampling in four columns that were

Figure 3. Baix LPS, Rhône Rift Valley, SE France. **(a)** Overview photo with white rectangles marking the positions of the close-up photos in panels **(b)**, **(c)**, **(d)** and **(e)**. **(b)** In situ carbonate nodules of horizon 5 BCk4 (∼ 850 cm depth). **(c)** Hydromorphic features of 7 Btg horizon (1199–1275 cm depth) of the basal Stagnic Luvisol. **(d)** Bleached root channel with lepidocrocite fringe (5–7 mm wide) in 7 Btg horizon (1227–1275 cm depth). **(e)** Vertically carved-in slots mark the positions of the sediment columns collected in boxes from 680 to 1360 cm depth for optically stimulated luminescence (OSL) screening (photos: Daniela Sauer, 2020).

slightly horizontally offset from one another (Fig. 3e). When the sampling shifted horizontally from one column to another, we used this chance to place the upper rim of the next lower flower box 10 cm above the depth of the lower rim of the previous flower box so that the block samples overlapped in these parts (partial columns 2, 3 and 4). Four partial sediment columns (subsections: 663–982 cm, 983–1072 cm, 1062–1150 cm, 1140–1368 cm) in 17 flower boxes represent one semi-continuous block sample, i.e. a vertical sediment column covering the lower ∼ 7 m of the profile wall. Empty spaces in the flower boxes were filled with paper wadding to prevent the sediment blocks from breaking during transport. The flower boxes with the samples were finally tightly wrapped with clingfilm to stabilise them and preserve the water content in the sediment samples. Laboratory codes of the box samples range from HDS-1802 (top) to HDS-1817 (bottom).

2.3 Methods

2.3.1 Granulometry, analysis of carbonate content and micromorphological analysis

Particle size distribution was measured by use of a laser diffraction particle size analyser (Beckman Coulter LS 13 320). First, soil organic matter of 10 g homogenised fine earth material (< 2 mm) was removed by adding 25 mL of 30 % H_2O_2 + 20 mL of deionised H_2O to the samples at 60 °C and allowing the samples to react for 12 h. This treatment was repeated until no visible reaction was observed (ISO 11277, 2020). Then, the samples were dispersed in 25 mL $Na_4P_2O_7 \times 10\ H_2O$ (0.1 mol^{-1}) + 200 mL deionised H_2O, shaken for 18 h in an overhead shaker and subsequently evaporated (ISO 11277, 2020). Carbonates were not removed because calcium carbonate grains constituted a substantial portion of the primary mineralogical and granulometric composition of the loess, which we did not want to lose. Samples containing high iron oxide contents (samples of Bt and Btg horizons) were additionally pre-treated with a solution of 4 % $Na_2S_2O_4$ + 0.3 mol L^{-1} $C_2H_3NaO_2$ to dissolve the iron oxides following ISO 11277 (2020). Samples were shaken for 12 h in an overhead shaker. They were then washed by adding deionised H_2O, centrifuging (5 min, 3500 rpm) and removing the supernatant by pipette. The treatment was repeated until the samples had completely lost their brownish colour. An aliquot of the pre-treated and dried sample was ultrasonicated for 30 s in deionised H_2O and inserted in the mixing chamber of the laser particle sizer. The arithmetic mean of three measurements of each sample was used to calculate the particle size distribution based on an optical model according to Mie theory with a complex refraction index (RI) of 1.56-i0.1 suitable for quartz (ISO 13320, 2020). The laser measurements yielded 116 particle size classes (0.04 to 2000 µm) which were grouped into particle size classes of clay, silt and sand (vol %). The limits of the classes were set according to Bosq et al. (2018, 2020b), i.e. at < 8 µm (clay), 8–56 µm (silt) and > 56 µm (sand). We chose the high limit for clay (i) because

it is commonly used to compensate for the known underestimation of clay content by laser diffraction (Konert and Vandenberghe, 1997; Beuselinck et al., 1998; Újvári et al., 2016) and (ii) because it allows for comparing the granulometric data of the Baix LPS with those of the Collias LPS. We used the U ratio (16–44 µm / 5.5–16 µm) to identify changes in sedimentary conditions during loess accumulation phases and the clay / silt ratio (< 8 µm / 8–56 µm) to identify phases of pedogenesis (Antoine et al., 2009; Újvári et al., 2016; Schulte and Lehmkuhl, 2018; Schulte et al., 2018). Carbonate content was determined by the gas-volumetric method using a Scheibler apparatus and calculated as calcium carbonate ($CaCO_3$) equivalents in weight percent (wt %; Blume et al., 2011). The soil blocks for micromorphological analysis were subjected to acetone exchange of the remaining pore water. Then, the blocks were impregnated with resin (Palatal), cut, glued on 28 mm × 48 mm glass slides and polished to a thickness of ∼ 25 µm. Micromorphological analysis was carried out in plane-polarised light (PPL) and cross-polarised light (XPL), using a Keyence VHX-7100 and/or VHX-E100 digital microscope, following the guidelines of Stoops (2021).

2.3.2 Luminescence screening

In recent years, various attempts have been made to profile sediment archives with luminescence techniques, also termed luminescence screening, i.e. in the case of optically stimulated luminescence, "OSL screening" (e.g. Sanderson et al., 2003; Burbidge et al., 2007; Sanderson and Murphy, 2010; Muñoz-Salinas et al., 2011; Kinnaird et al., 2012; Bateman et al., 2015; Portenga and Bishop, 2016; May et al., 2018; Fitzsimmons et al., 2022).

In contrast to conventional luminescence dating, luminescence screening involves minimal sample preparation, measurement of a few aliquots (usually one to three) and/or considerably shortened measurement procedures. The profiling maps the brightness (sensitivity) of one or more luminescence signals, for example, blue-light-stimulated luminescence (BLSL), infrared-stimulated luminescence (IRSL) or thermally stimulated luminescence (TL), e.g. along a sediment core (changes with depth) or in two dimensions across a profile wall. The use of a portable luminescence reader during fieldwork (cf. Scottish Universities Environmental Research Centre (SUERC) portable OSL reader; Sanderson and Murphy, 2010) may help to optimise the positions of OSL samples and to understand the stratigraphy of a sediment archive if the luminescence sensitivities correlate with different sediment units (Sanderson et al., 2003; Muñoz-Salinas et al., 2011). Among others, the sensitivity may reflect the characteristics of the minerals (usually quartz and feldspar), the amount of the palaeodose accumulated over time since the last exposure to daylight and varying local dose rates within the sediment deposit. However, in order to relate the luminescence counts gained by a portable OSL reader to the natural dose accumulated by a sample since the last sediment reworking, the sample material needs to be artificially irradiated, e.g. by an external gamma source, to allow for comparison of the natural signal of a sample to that received after the irradiation with a calibrated source (Sanderson and Murphy, 2010). Further, some sort of dose rate estimation is required to transform the palaeodose estimates into a rough age estimate. Luminescence profiling has been successfully applied in different sedimentary environments, such as colluvium and alluvium (Muñoz-Salinas et al., 2014; Portenga and Bishop, 2016), coastal sand dunes (Bateman et al., 2015), swamp deposits (May et al., 2018), and loess (Fitzsimmons et al., 2022), including deposits at archaeological and prehistoric sites influenced by humans (Sanderson et al., 2003; Burbidge et al., 2007).

Luminescence profiling can be improved by applying the single-aliquot regeneration (SAR) protocol (Murray and Wintle, 2000) to closely spaced samples that are minimally prepared in the dark luminescence laboratory for measurements on a conventional automated luminescence reader, equipped also with a calibrated radiation source. Burbidge et al. (2007) and Kinnaird et al. (2012) applied a simplified SAR protocol to different mineral and grain size fractions of their samples, while May et al. (2018) measured one cycle of a complete SAR protocol (the natural luminescence signal, L_n, and the OSL signal received after an applied test dose, T_n) without grain size separation. L_n/T_n values were further normalised by the dose rates, which varied considerably along the profile. Fitzsimmons et al. (2022) used IRSL from unprepared bulk material of Rhine Valley loess read out at 50 °C (IR_{50}). Again, the luminescence signal was normalised by a test dose signal (L_n/T_n). The variation in the test-dose-normalised signal sensitivity was regarded as a proxy for varying source areas of the loess deposits. Thus, approaches to luminescence screening do not follow a strict protocol and are adjusted according to the aims of a study.

Luminescence screening "age estimates"

In this study, we performed luminescence screening to support the stratigraphy based on detailed field observation, hypothesising that the lower ∼ 7 m of the Baix LPS reflect the Eemian to Middle Pleniglacial palaeoenvironmental changes. Therefore, we collected data on the luminescence sensitivity, the (approximate) palaeodoses and the dose rates. In addition, we applied a sensitivity approach following Fitzsimmons et al. (2022) but using the coarse fraction and performing an additional step for inter-aliquot normalisation to obtain a proxy indicating the likely provenance of the material. Here, we give a brief outline of the procedure, while a detailed description is given in the first part of the Supplement ("Methods – Luminescence screening").

A semi-continuous sequence of material was collected from the lower ∼ 7 m of the Baix LPS in 16 vertically aligned boxes (laboratory codes of the OSL box samples are HDS-

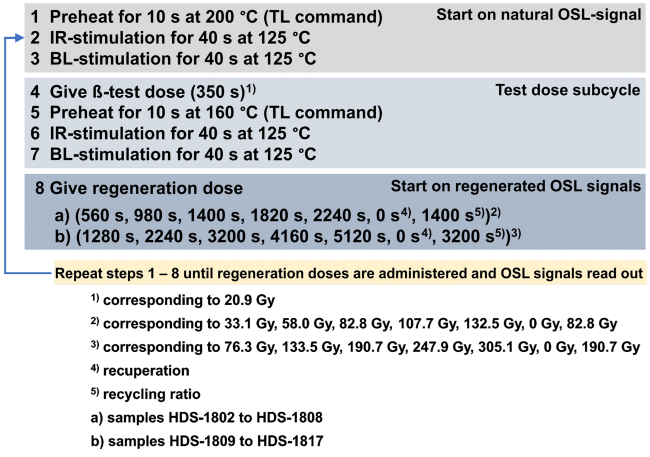

Figure 4. pIR-BLSL SAR protocol applied to minimally prepared polymineral coarse grains from 126 miniature (1 cm^3) subsamples.

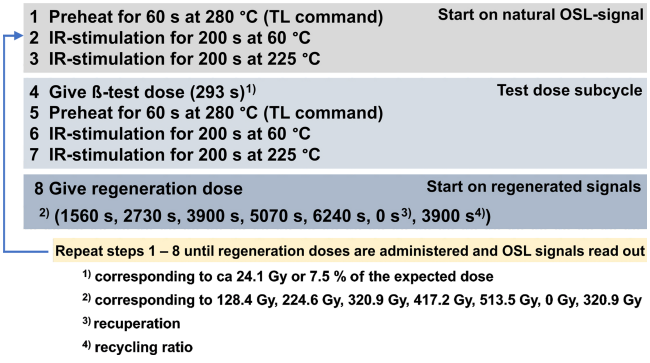

Figure 5. $pIR_{60}IR_{225}$ SAR protocol applied to minimally prepared polymineral coarse grains from 126 miniature (1 cm^3) subsamples.

1802 (top) to HDS-1817 (bottom) (cf. Sect. 2.2.2). In the dark luminescence laboratory, up to eight ca. 1 cm^3 small subsamples (A–H) were extracted at intervals of 5 cm from each box sample (altogether 126 subsamples). Additional material was taken for water content and radionuclide determination, both needed for calculating an effective dose rate. Minimal sample preparation included wet sieving (125 µm mesh size) and preparation of small aliquots (a few hundred grains) from the retained polymineral coarse-grain fraction (> 125 µm).

To provide a time frame, we applied the SAR protocol establishing dose–response curves with several test-dose-normalised regeneration-dose points (L_x/T_x), including dose points for testing the recuperation and recycling ratio, once with a BLSL protocol (Murray and Wintle, 2000) after IR stimulation (pIR-BLSL) and signal detection in the UV (Hoya U340) and once with a post-infrared (at 60 °C) infrared (at 225 °C) protocol ($pIR_{60}IR_{225}$) (Thomsen et al., 2008) with detection of the blue emission around 410 nm (through interference filter CH-30D410-44.3). All measurements were performed on two automated luminescence Risø reader models, TL/OSL DA15 and TL/OSL DA20 (an update of TL/OSL DA15), respectively (Lapp et al., 2012, 2015). The protocols are illustrated in Figs. 4 and 5.

We aimed to extract a quartz-dominated signal with the pIR-BLSL protocol and a potassium-feldspar-dominated signal with the $pIR_{60}IR_{225}$ protocol. For adapting the pIR-BLSL and the $pIR_{60}IR_{225}$ protocols to the Baix samples, we performed a series of tests, including D_e-range tests, dose recovery tests, normalisation dose tests ($pIR_{60}IR_{225}$ protocol only) and tests of anomalous fading. Thus, our OSL-screening approach contained all relevant preparatory measurement steps needed for elaborated SAR OSL dating. In contrast to proper OSL dating, however, the D_e measurements were performed on only three aliquots per subsample for the pIR-BLSL approach and one aliquot per subsample for the $pIR_{60}IR_{225}$ protocol in order to save measurement time. For dose rate assessment, radionuclide determination was performed with the novel μDose system (Tudyka et al., 2018, 2020; Kolb et al., 2022) on six samples regarded as representative of the Baix sediments and palaeosols. Assuming radioactive equilibrium, the radionuclide concentrations were transformed to dose rates (Guérin et al., 2011), while the cosmic dose rate was calculated with the R package "Luminescence" (Kreutzer et al., 2012). Following standard procedures, we assumed an internal potassium content of 12.5 ± 1.25 wt % for the $pIR_{60}IR_{225}$ protocol, a values of 0.1 ± 0.02 for the $pIR_{60}IR_{225}$ approach (Kreutzer et al., 2014) and 0.035 ± 0.02 (Lai et al., 2008) for the pIR-BLSL approach and water content as suggested by Sauer et al. (2016) and applied to the Collias LPS by Bosq et al. (2020b). While our OSL "age estimate" calculation relies on 126 D_e measurements for the $pIR_{60}IR_{225}$ protocol and the triple number of D_e measurements for the pIR-BLSL protocol, a mean effective dose rate was used for each of the two SAR protocols. Due to the reduced number of aliquots used for D_e determination and the use of a representative mean effective dose rate for each of the two SAR approaches, we called them "age estimates" and put them into quotation marks. We consider our luminescence screening approach for deriving OSL "age estimates" adequate for testing the field hypothesis of whether the lower ~ 7 m of the Baix LPS contains an Eemian to Middle Pleniglacial record. We will additionally perform OSL dating on selected samples in future studies.

Luminescence sensitivity

Varying luminescence sensitivities in a loess profile may serve as a proxy for different source areas or materials (Fitzsimmons et al., 2022). We compared the IR signal of the aliquots measured with the pIR-BLSL protocol to the subsequently readout BLSL signal, using all measured test dose signals (T_x) for this procedure. For determining the luminescence sensitivities, first, the T_x signals of a complete SAR measurement (eight measurement points) were averaged for

each aliquot (T_{x_mean} of an aliquot) before a mean with the standard error of the three aliquots of each subsample was calculated (T_{x_mean} of a subsample). Finally, the ratio of the signals of the two stimulations was derived (T_{x_IR}/T_{x_BLSL}). While samples with a dominant IR signal may point to the predominance of feldspar (emitting in the UV), the dominance of a BLSL signal could indicate the predominance of quartz in the polymineral coarse grains. Thus, larger values (ratios) would point to more feldspar emitting around 340 nm and smaller ratios to a quartz dominance emitting in that range.

3 Results

3.1 General overview of the Baix LPS

The overall 13.7 m thick Baix LPS was subdivided into 19 horizons, developed in (mostly reworked) loess and soil sediments that overlie slope deposits with a large share of rock fragments from local bedrock (Table 1). Four levels of soil formation were identified, in the following termed "Holocene soil", "upper interstadial palaeosol", "lower interstadial palaeosol" and "interglacial palaeosol complex". Several erosional discontinuities were observed, e.g. above the 7 Btg and 5 Bw2 horizons. Various forms and sizes of secondary carbonate accumulation, i.e. pseudomycelia, hard nodules and soft carbonate concentrations, were observed (Table 1, Fig. 3b). All horizons showed abundant bioturbation features such as root channels and earthworm burrows, which make it a challenge for luminescence dating.

3.1.1 Granulometry and carbonate contents

The mean particle size distribution in the lower 7 m of the Baix LPS included 26 vol % clay, 55 vol % silt and 19 vol % sand. The palaeosol horizons exhibited the highest clay contents with up to 30 vol % clay, whereas the only slightly weathered loess horizons showed the highest silt (60 vol %) and sand (26 vol %) contents. The main mode was in the coarse silt fraction (34 µm), and the mean particle size was in the range 29–41 µm, with an arithmetic mean of 33 µm. Rock-fragment contents ranged from 0 wt % up to 80 wt %. U ratios were in the range 1.55–2.59, exhibiting maxima in the only slightly weathered loess deposition phases and decreasing in the palaeosol horizons (Fig. 11). Clay / silt ratios showed an opposite trend, overall ranging between 0.35 and 0.58. The least weathered loess (5 Ck2 horizon) contained 23 wt % $CaCO_3$, which was the maximal measured $CaCO_3$ content. The lowest $CaCO_3$ content (0.3 wt %) was found in the 7 Bt1 horizon, belonging to the interglacial palaeosol complex.

3.1.2 Micromorphology

The groundmass of the three thin sections of the Baix LPS displayed quartz and carbonate grains with lower quantities of feldspars and biotite. All horizons showed calcitic and/or textural pedofeatures. They had massive (Fig. 6b) to weakly subangular blocky (Fig. 6c) microstructures and calcitic crystallitic (Fig. 7d) to stipple-speckled and porostriated (Fig. 7f) b-fabrics. Voids mainly included channels, chambers and vughs (Fig. 6a–c). The number and size of orthic and disorthic Fe nodules increased with depth (Fig. 6a–c). Calcite earthworm granules and/or calcified root cells were observed in all three thin sections (Fig. 7c–d).

3.2 Detailed characterisation of the lower 7 m of the Baix LPS

3.2.1 Basal interglacial palaeosol complex

The basal interglacial palaeosol complex of the Baix LPS was classified as a Stagnic Luvisol (IUSS Working Group WRB, 2022), of which a Btg horizon and two underlying Bt horizons were preserved (Table 1), all characterised by an intense reddish-brown to orange-brown colour and massive to subangular blocky structure. This palaeosol complex exhibited the highest clay contents (25 vol %–37 vol %) and lowest silt contents (45 vol %) of the investigated part of the Baix LPS. Thereby, the slightly carbonated (8 wt %) 8 Bt2 horizon had the highest rock-fragment content (80 wt %) and the highest clay content (37 vol %), although no clay coatings were observed. The overlying 7 Bt1 and 7 Btg horizons had clay contents of up to 30 vol % and displayed clay coatings that were observed both in the field and in the thin sections. Both disturbed and/or relocated clay coatings (Fig. 6c) and undisturbed clay and clay–silt coatings along voids, indicating in situ clay migration (Fig. 7e–f), were identified under the microscope. The 7 Bt horizon contained up to 12 wt % rock fragments (in its basal part), whereas the overlying 7 Btg horizon had no rock fragments. It showed in situ stagnic properties, i.e. bleached root channels and prominent undisturbed Mn and Fe concentrations and coatings (Fig. 3c–d).

3.2.2 Lower and upper interstadial palaeosols

The lower interstadial palaeosol was represented by the decarbonated bipartite brown 6 Bw3 horizon with massive structure. The horizon was marked by increased clay (27 vol %–29 vol %) and decreased silt (52 vol %–57 vol %) and sand (15 vol %–19 vol %) contents. It contained up to 1 wt % of rock fragments. The lower part of the bipartite horizon displayed faint clay coatings and loess-infilled former root channels (Table 1). The upper interstadial soil was represented by the brown decarbonated 5 Bw2 horizon and the underlying 5 Bk2 and 5 BCk4 horizons. The 5 Bw2 horizon had massive to weak subangular blocky structure. Its clay (27 vol %–30 vol %), silt (52 vol %–54 vol %) and sand (16 vol %–21 vol %) contents were similar to those of the

Table 1. Horizon designations and characteristics of the horizons of the Baix LPS according to the *Guidelines for soil description* (FAO, 2006) and interpretation with respect to sedimentary and pedogenic processes. Soil colour is given according to Munsell Soil Colour Charts (moist). Abbreviations and definitions: PM, pseudomycelia; HC, hard carbonate nodules; HHC, hard hollow carbonate nodules; SC, soft carbonate nodules; very small carbonate nodules, ca. 1 to 5 mm in diameter (∅); small carbonate nodules, ca. 0.5 to 1.5 cm ∅; medium-sized carbonate nodules, 1.5 to 5 cm ∅; large carbonate nodules, ≥ 5 cm ∅; WE, earthworm channels; WC, earthworm casts; Mn, manganese.

No.	Horizon	Depth (cm)	Subdivision (cm)	Main characteristics	Interpretation	
1	Ah	0–20		disturbed surface; clear smooth lower boundary; dark-brown colour (10 YR 3/2); fine and medium granular structure; many WC	colluvial deposit, Holocene Cambisol	Holocene soil
2	Bw1	20–65	20–30	clear smooth lower boundary; dark-brown colour (10 YR 4/4); moderate fine and medium subangular blocky structure; many WE, burrows, infilled small burrows		
			30–45	gradual smooth lower boundary; intense brown colour (10 YR 4/6); moderate fine and medium subangular blocky structure; PM; many WE, burrows, infilled small burrows		
			45–65	gradual smooth lower boundary; brown colour (10 YR 5/6); moderate medium subangular blocky structure; PM; many WE, infilled small burrows		
3	Bk1	65–95		gradual smooth lower boundary; brown colour (10 YR 5/4); weak medium subangular blocky structure; PM; small few HC, HHC; common WE		
4	BCk1	95–240	95–200	gradual smooth lower boundary; light-brown colour (10 YR 6/4); massive structure; PM, small few HC, HHC	slope-washed loess with varying degrees of pre-weathering	Loess
			200–240	gradual smooth lower boundary; brown colour (10 YR 5/4); massive structure; small HC, SC		
5	Ck1	240–374	240–280	gradual smooth lower boundary; light-brown colour (10 YR 6/4); massive structure; few PM, small HC; mollusc-shell fragments		
			280–374	gradual smooth lower boundary; yellowish-brown colour (10 YR 6/3); massive structure; few PM, few very small HC; very few very fine soft Mn concentrations		
6	CBk	374–500		gradual smooth lower boundary; greyish-brown colour (10 YR 5/3); massive structure; long PM, very small HC; very few very fine spheroidal soft Mn concentrations; charcoal pieces		
7	2 BCk2	500–570/590		gradual smooth lower boundary; light-brown colour (10 YR 5/4); strong massive structure; PM, few small HC; very few very fine spheroidal soft MN concentrations		
8	3 BCk3	570/590–700		gradual smooth lower boundary; light-brown colour (10 YR 5/4); strong massive structure; PM, few small in situ HC; very few very fine round soft Mn concentrations		
9	4 BCk/Bw	700–735		clear to gradual smooth lower boundary; light-brown colour (10 YR 5/6); strong massive structure; PM, very few small HC; very few very fine spheroidal soft Mn concentrations	mixture of reworked soil sediment and loess	
10	5 Bw2	735–775		gradual smooth lower boundary; brown colour (10 YR 4/6); massive to weak coarse subangular blocky structure; few PM, very few very small HC; loess-coloured infillings in WE; contains small rock fragments	truncated Bw horizon of Cambisol	Upper interstadial palaeosol
11	5 Bk2	775–820		gradual smooth lower boundary; brown colour (10 YR 4/6); massive to weak coarse subangular blocky structure; PM, few small in situ HC	slightly weathered, lower in situ horizon of Cambisol	
12	5 BCk4	820–853		gradual smooth lower boundary; brown colour (10 YR 5/4); strong massive to subangular blocky structure; PM, many large in situ HC (up to 8–15 cm long, 4–6 cm width); contains small rock fragments	In situ carbonate accumulation horizon of Cambisol	

Table 1. Continued.

No.	Horizon	Depth (cm)	Subdivision (cm)	Main characteristics	Interpretation	
13	5 Ck2	853–995	853–915	gradual smooth lower boundary; light-brown colour (10 YR 6/4); strong massive structure; few PM, HC; few incompletely infilled former root channels; many recent root channels; rock fragments	slope-washed loess with varying degrees of pre-weathering	Loess
			915–995	gradual smooth lower boundary; yellowish-brown colour (10 YR 6/3); strong massive structure; few PM, HC; darker-brown sediment-filled former root channels; few recent root channels; small rock fragments		
14	5 BCk5	995–1080		clear smooth lower boundary; brown colour (10 YR 5/4); massive structure; very few very small in situ HC; very few very fine spheroidal soft Mn concentrations; small rock fragments		
15	6 Bw3	1080–1155	1080–1120	gradual smooth lower boundary; brown colour (10 YR 4/6); massive structure; very few very fine round soft Mn concentrations; small rock fragments	Bw horizon developed in a mixture of reworked soil sediment and loess	Lower interstadial palaeosol
			1120–1155	gradual smooth lower boundary; brown colour (10 YR 4/6); massive structure; very few faint clay coatings; few very small in situ HC; very few very fine spheroidal soft Mn concentrations; loess-infilled former root channels; small rock fragments		
16	6 BCk/Btg	1155–1199	1155–1178	clear smooth lower boundary; brown colour (10 YR 5/8); massive structure; few small HC; few very fine spheroidal Mn concentrations; rock fragments	mixture of reworked soil sediment and loess	Loess
			1178–1199	clear smooth lower boundary; yellowish-brown colour (10 YR 5/8) and reddish-brown colour (7.5 YR 5/6); weak massive to subangular blocky structure; very few faint to distinct clay coatings; SC, few small HC; common fine to medium irregular flat soft Mn concentrations; lower part with iron oxide mottles and depletion zones	
17	7 Btg	1199–1315	1199–1227	clear to gradual smooth lower boundary; reddish-orange-brown colour (7.5 YR 4/6); weak coarse and very coarse subangular blocky structure; few distinct clay coatings; few in situ HC; many fine to medium irregular flat soft Mn concentrations; iron oxide mottles and depletion zones	Bt and Btg horizons of Stagnic Luvisol (subdivision based on the intensity of hydromorphic features) developed in reworked soil sediment	Interglacial palaeosol complex
			1227–1275	clear to gradual smooth lower boundary; reddish-orange-brown colour (7.5 YR 5/8); weak coarse and very coarse subangular blocky structure; common distinct clay coatings; few in situ HC; many fine and medium spheroidal soft Mn concentrations; iron oxide mottles and depletion zones; bleached root channels seamed by Lepidocrocite hems (5–7 mm thick); depth where hydromorphic features are most prominent		
			1275–1315	gradual smooth lower boundary; reddish-orange-brown colour (7.5 YR 5/8); weak coarse and very coarse subangular blocky structure; common distinct clay coatings; many very fine and fine spheroidal soft Mn concentrations; iron oxide mottles and depletion zones; bleached root channels seamed by Lepidocrocite hems (2–3 mm thick); root channels incompletely filled with sediment		
18	7 Bt1	1315–1360		abrupt smooth lower boundary; reddish-brown colour (7.5 YR 5/6); weak coarse and very coarse, subangular blocky structure; few distinct clay coatings; many very fine spheroidal soft Mn concentrations; few WE filled with WC; rock fragments		
19	8 Bt2	1360–1370		clear wavy lower boundary; reddish-brown colour (7.5 YR 6/6); strong massive structure; weathered (soft) and unweathered fragments	mixture of reworked soil sediment, loess and local rock debris	
20	Cw	1370+		debris of Lower Cretaceous limestone and marl and of basalt	slope deposit of local rock debris	

6 Bw3 horizon of the lower interstadial palaeosol. The 5 Bw2 horizon of the upper interstadial soil contained up to 7 wt % of rock fragments. Under the microscope, rounded microaggregates, dusty silt-clay coatings along pores, in situ Fe nodules, partially decomposed root remains, and calcite earthworm granules were observed (Figs. 6b, 7a–b). The 5 Bk2 and 5 BCk4 horizons underlying the 5 Bw horizon were characterised by reprecipitation of the carbonates leached from the 5 Bw horizon, forming large in situ carbonate nodules. The largest carbonate nodules (8 to 15 cm long, 4 to 6 cm wide) were found at 810–860 cm depth (Fig. 3b). The carbonate nodules were yellowish brown; contained silicate grains including rock fragments; and displayed a porous, homogenous structure.

3.2.3 Erosional discontinuities and characteristics of the slightly to moderately weathered loess

Major erosional discontinuities were observed above the interglacial palaeosol complex and above the upper interstadial palaeosol. Both of these discontinuities were followed by a layer of mixed sediment, containing clearly recognisable portions of reworked palaeosol material and only slightly weathered loess (6 BCk/Btg and 4 BCk/Bw). These mixed layers displayed high rock-fragment contents (up to 20 wt %). The parts of the Baix LPS where the sediment was only slightly to moderately weathered (5 BCk5, 5 Ck2, 5 BCk 4, 5 Bk2, 3 BCk3) had yellow-brown (Ck), light-brown (BCk) and brown (Bk) colours; had massive to weak subangular blocky structure; and contained 5 wt %–22 wt % $CaCO_3$, reflecting their different weathering degrees (Table 1). The least weathered 5 Ck2 horizon displayed the highest silt content (60 vol %), high sand content (24 vol %) and the lowest clay content (20 vol %) of the investigated part of the Baix LPS. Otherwise, the slightly to moderately weathered loess was composed of 49 vol %–59 vol % silt, 16 vol %–26 vol % sand and 21 vol %–28 vol % clay. Rock-fragment contents were in the range of 0 vol %–6 wt %. Abundant bioturbation features were observed in the thin sections, including calcite earthworm granules, calcified root cells and former root channels coated by micritic carbonate precipitates (Figs. 6b, 7c–d).

3.3 Luminescence screening results

Examples of pIR-BLSL and $pIR_{60}IR_{225}$ shine-down, dose–response curves and graphical results of the fading tests are given in the second part of the Supplement ("Results – Luminescence screening") (all g values normalised to 2 d). While four aliquots measured with the pIR-BLSL protocol showed g values, which within error margins agreed with zero, eight aliquots exhibited g values pointing to fading. For the $pIR_{60}IR_{225}$ protocol, four aliquots exhibited g values which conform with zero, while the other four aliquots showed g values above zero (mean of all eight aliquots 6.45 ± 1.16). As this is not expected for pIR-IR measurements (Thomsen et al., 2008), we eliminated the prompt readouts for g-value determination. This produced a mean g value over all eight aliquots of 1.24 ± 2.48, conforming with zero (no fading). Therefore, we assumed that the larger g values for the $pIR_{60}IR_{225}$ protocol were measurement artefacts (cf. Thiel et al., 2011). Such measurement artefacts may be produced if prompt readouts are included in fading measurements and no minimum time after irradiation and preheating is considered (see final public response to discussion of Kadereit et al., 2020). As no correlation between the size of a D_e of an aliquot and its g value was observed, we expect the $pIR_{60}IR_{225}$ protocol to deliver reliable data.

The results of the effective dose rate determination for the six selected samples are presented in Fig. 8. They show a relatively narrow spread, justifying the use of a mean effective dose rate for the OSL screening. For pIR-BLSL measurements, supposed to sample quartz, the effective dose rates ranged between 2.43 ± 0.18 and 2.93 ± 0.23 Gy ka^{-1} (dark-blue symbols), giving a mean value of 2.80 Gy ka^{-1} (blue line). For $pIR_{60}IR_{225}$ measurements, likely sampling potassium feldspar, the effective dose rates range between 3.52 ± 0.19 Gy ka^{-1} and 4.15 ± 0.24 Gy ka^{-1} (red symbols), providing a mean value of 3.98 Gy ka^{-1} (red line). These values were used for OSL "age estimate" calculation. For the lowermost silt loam sample, a higher water content was also assumed (light-blue and yellow symbols) for dose rate assessment, accounting for its hydromorphic features. While for "age estimate" calculation, D_e errors and beta source calibration errors were taken into account, only the mean values of the dose rate without assuming an error were considered. Thus, the OSL screening gives an idea of the course of the burial doses along the lower 7 m of the Baix LPS, divided by an effective dose rate regarded as representative, to produce a profile of approximate "age estimates" (Fig. 9). A graph summarising OSL "age estimates" block-wise for each of the 16 boxes HDS-1802 to HDS-1817 following the central age model approach of Galbraith et al. (1999) is provided in Fig. S5 in the second part of the Supplement. Throughout the investigated part of the profile, pIR-BLSL "age estimates" are smaller than $pIR_{60}IR_{225}$ "age estimates".

While the course of "age estimates" gained with both the pIR-BLSL and the $pIR_{60}IR_{225}$ protocol shows a trend of increasing data values from top to ca. 12.3 m depth, surprisingly, the values do not increase further below that depth for the pIR-BLSL protocol. Further, several aliquots measured with the pIR-BLSL SAR protocol show "age estimates" younger than the Last Glacial Maximum (LGM) limit (cf. yellow line in Fig. 9), which is not logical for loess deposits, especially not at depths several metres below the ground level. Although the incorporation of quartz grains from the surface and younger deposits by bioturbation cannot be excluded, with quartz being bleachable faster than feldspar (Godfrey-Smith et al., 1988), this assumption does not seem appropriate as an explanation for the comparably young(er)

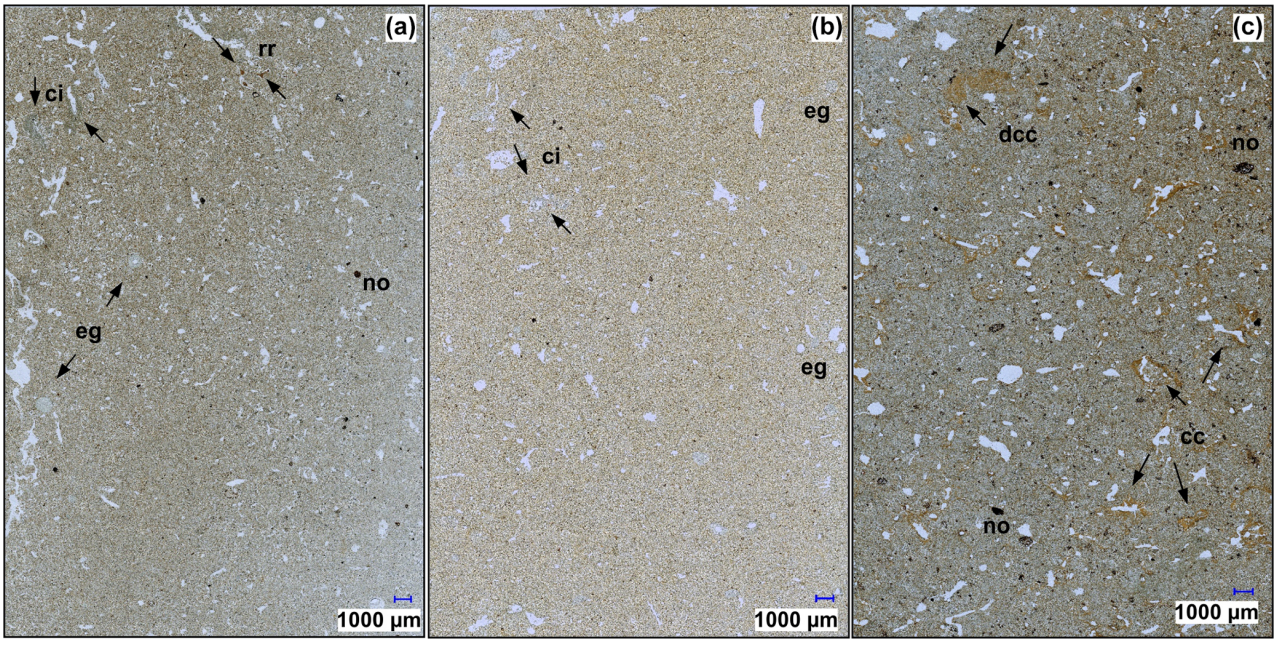

Figure 6. Photos of whole thin sections (3 cm × 4 cm) of the Baix LPS, Rhône Rift Valley, SE France. **(a)** Decarbonated 5 Bw2 horizon (755–763 cm): weakly subangular blocky microstructure (in places crumbly, channel microstructure). Voids: channels and vughs. Voids impregnated with calcite hypo- and quasi-coatings, channel infillings, and porous and dense rounded microaggregates. Typic, rounded and digitated elongated disorthic Fe / Mn nodules and digitated Fe / Mn impregnations. Calcite earthworm granules with clay–silt capping and root residues. **(b)** 5 Ck2 horizon (935–943 cm depth): massive, vugh microstructure. Voids: vughs and channels, some infilled with dense rounded microaggregates, partially with calcite hypocoatings. Few small Fe / Mn nodules. Calcite earthworm granules. **(c)** Decarbonated 7 Bt1 horizon (1335–1343 cm depth): weak subangular blocky, crumbly microstructure. Voids: channels, vughs and chambers. Some channels infilled with porous to dense microaggregates. Voids with limpid orange (relocated) clay coatings. Abundant round, digitated, elongated disorthic Fe / Mn nodules; large (∅ 380 µm) Fe impregnations. Abbreviations: cc, clay coating; ci, calcite impregnation; dcc, disturbed clay coating; eg, calcite earthworm granule; no, Fe nodules; rr, root residues.

"age estimates" produced by the pIR-BLSL SAR protocol. In general, we suppose that the pIR-BLSL "age estimates" are less reliable than the $pIR_{60}IR_{225}$ "age estimates" produced by our OSL-screening approach. We assume that the IR depletion of the polymineral coarse grains was too incomplete to get a more or less "pure" BLSL signal from quartz. It is likely that the polyminerals emitted an unstable UV emission from feldspar, especially as preheating and pIR-BLSL readout occurred at significantly lower temperatures and for considerably shorter times than for the $pIR_{60}IR_{225}$ protocol. This assumption agrees with the partly considerable g values observed by the fading tests. For these reasons, we disregard the age assessments associated with the pIR-BLSL measurements and only consider the $pIR_{60}IR_{225}$ "age estimates" for the discussion. The derived "age estimates" of the OSL screening are tentatively reflected against the MIS as defined by Lisiecki and Raymo (2005) (Fig. 9). As the MIS stratigraphy rather reflects global climate changes, we correlated our OSL "age estimate" results with stadial and interstadial phases derived from European terrestrial (LPSs, pollen and lacustrine sequences) archives (Woillard, 1978; Beaulieu and Reille, 1992; Guiter et al., 2003; Haesaerts et al., 2016).

OSL sensitivity values

The OSL sensitivity values (IRSL / pIR-BLSL ratios) originate from coarse-grain separates and therefore do not represent the far-transported aeolian main component of the LPSs but rather accessories. They ranged between ca. −0.5, likely pointing to subdued contribution from feldspar, and ca. +1.5 (Fig. 10), likely pointing to an increased contribution from feldspar (or feldspar having a stronger signal in the UV range if the depletion of the OSL signal was insufficient by the IR stimulation).

Low values of around −0.5 occurred in the lowermost horizon, 7 Bt1. The largest concentration of values around 1.5 occurred in the overlying 7 Btg horizon. "Balanced" values scattering closely around 1 occurred in the overlying horizons, i.e. 6 BCk/Btg to 5 Ck2. Values alternating between these two extremes are observed in the 5 Ck2 to 3 BCk3 horizons. Thus, the OSL screening seemed to serve as a proxy for variations in the sediment sources, as suggested by Fitzsimmons et al. (2022), and supported a subdivision into four parts marked in Fig. 10.

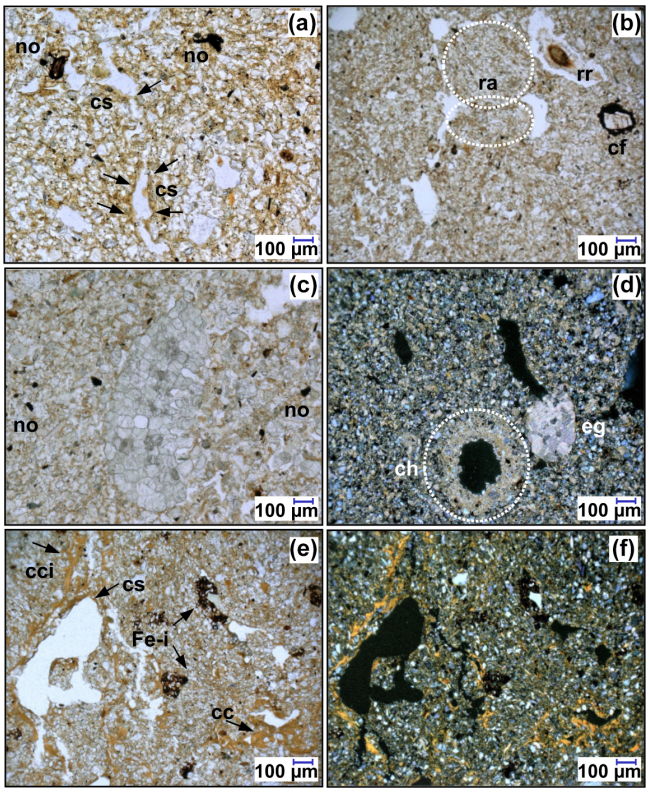

Figure 7. Photomicrographs of thin sections of the Baix LPS, Rhône Rift Valley, SE France. **(a)** Brown clay–silt coatings along voids in the 5 Bw2 horizon (755–763 cm) and elongated and digitated Fe / Mn nodules (plane-polarised light; PPL). **(b)** Rounded (bioturbated) aggregates in the 5 Bw2 horizon (755–763 cm) with root residues and in situ weathered calcite fragment. **(c)** Calcified root cells in 5 Ck2 horizon (935–943 cm depth) with elongated anorthic Fe / Mn nodules and digitated Fe impregnations (PPL). **(d)** Subrounded (relocated) calcite earthworm granule and calcite hypocoatings along voids in the carbonatised groundmass of the 5 Ck2 horizon (935–943 cm depth) (cross-polarised light; XPL). **(e)** Limpid orange clay and dusty-brown silt coatings and infillings with disorthic Fe impregnations in the 7 Bt1 horizon (1335–1343 cm depth) (PPL). **(f)** Same area as panel **(e)** under XPL, Stipple-speckled, partly porostriated b-fabric of the 7 Bt1 horizon (1335–1343 cm depth). Abbreviations: cc, clay coating; cci, clay coating infilling; cf, calcite fragment; ch, calcite hypocoatings; cs, clay–silt coating; eg, calcite earthworm granule; Fe-i, Fe impregnation; no, nodule; ra, rounded aggregate; rr, root residues.

4 Discussion – Eemian to Middle Pleniglacial evolution of the Baix LPS and corresponding palaeoenvironmental conditions

4.1 The Eemian and early glacial period

The basal interglacial palaeosol complex was composed of three horizons, whereby the lowermost horizon (8 Bt2) had developed not in loess but in a slope deposit with high content of local rock debris. Its difference in parent material is also reflected in its different OSL sensitivity ratio (Fig. 10). Most likely, its high clay content was partially inherited from the pre-weathered slope deposit. The reddish-brown colour and the presence of in situ clay coatings in the overlying 7 Bt1 horizon suggested warm and at least seasonally humid conditions. Relocated aggregates and broken clay coatings in the matrix indicated intense bioturbation. The uppermost reddish- to orange-brown 7 Btg horizon of the basal interglacial palaeosol complex showed similar characteristics to the 7 Bt1 horizon but in addition exhibited strong stagnic properties (Table 1). The sediment in which these two upper horizons of the interglacial palaeosol complex had developed yielded penultimate-glacial to Eemian "age estimates" and exhibited an above-average OSL sensitivity ratio over the entire thickness of the two horizons. Thus, the sediment was clearly different from the last-glacial slope-wash loess that made up the overlying part of the Baix LPS. We thus interpreted the basal interglacial palaeosol complex as an Eemian palaeosol complex, developed in slope deposits with predominant penultimate-glacial loess component, corresponding to the basal red palaeosol in the Collias LPS ∼ 100 km further south (Bosq et al., 2020b). The declining OSL "age estimates" at the base appear to indicate an age reversal. However, in the simplified approach applied in the present study, a common dose rate was assumed for all samples, neglecting the stagnic conditions that clearly prevailed for some time at the base of the Baix LPS, and thus reducing the effective dose rate and increasing the "age estimates" accordingly. Assuming an increased water content (Fig. 8), the "age estimate" at the base would be in agreement with the expected stratigraphy. This issue needs to be addressed in more detail in future studies with more sophisticated OSL approaches. The apparent Eemian "age estimates" for the lower and central part of the 7 Btg horizon may be owed to reworking by short-distance slope-wash processes. The uppermost part of the 7 Btg horizon may have even developed in a younger deposit, possibly reworked and deposited during the late early glacial period (e.g. Mélisey I, with subsequent pedogenesis during St Germain I), as incorporation of soil peds eroded from the underlying horizon and re-sedimentation of insufficiently bleached material could lead to age overestimation. Possible reworking phases correlate most likely with the stadials Mélisey I and Mélisey II (MIS 5d, 5b; Herning, Rederstall (Guiter et al., 2003); St Nicolas, Saint Haon (Reille et al., 2000)) of the early glacial period (Beaulieu and Reille, 1984b; Guiot et al., 1993). The subsequent periods of landscape stability, reflected in the Baix LPS, again by soil formation, possibly correlate with the interstadials St Germain I and St Germain II (MIS 5c, 5a; Amersfoort–Brørup, Odderade (Guiter et al., 2003); St Geneys 1, St Geneys 2 (Reille et al., 2000)) (Beaulieu and Reille, 1984b).

Thus, we assume that the basal Eemian palaeosol complex in the Baix LPS started to develop under conditions of dry, warm summers and wet, mild winters, leading to the 7 Bt1 and 8 Bt2 horizons. After a period of reworking (dur-

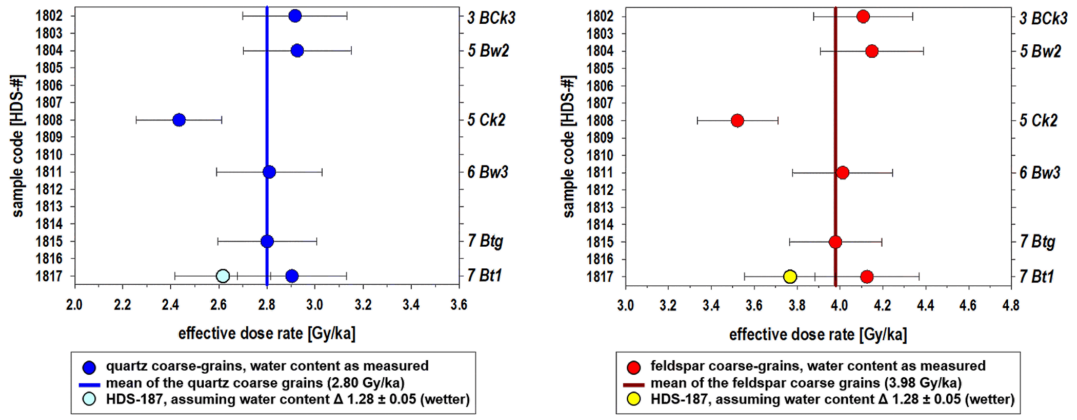

Figure 8. Effective dose rates determined for the six selected samples subjected to measurements with the μDose device to determine the radionuclide concentrations. The error bars take the water contents of the subsamples into account, expressed as moist weight / dry weight = 1.17 ± 0.05. Because of stagnic properties in the basal part of the Baix LPS, we additionally calculated effective dose rates for wetter conditions (1.28 ± 0.05) for sample HDS-1817. The water content estimates are based on Sauer et al. (2016).

ing Mélisey I and/or Mélisey II), soil formation continued into the middle and late early glacial period in the reworked material of the Eemian soil. Eemian Luvisol formation and subsequent truncation and/or reworking are well known from European LPSs (Antoine et al., 2001, 2009, 2016; Günster et al., 2001; Haesaerts et al., 2016). However, early glacial palaeosol horizons in mid-latitude European LPSs generally reflect drier conditions compared to the Eemian conditions (Mosbacher Humus zones) (Antoine et al., 2001, 2016; Schirmer, 2016), whereas in Mediterranean LPSs, more humid conditions seem to be reflected by polygenetic Eemian to early glacial palaeosol complexes (Günster et al., 2001; Ferraro, 2009; Wacha et al., 2011). Within the Rhône Rift Valley, the Eemian palaeosol complex in the Baix LPS is in accordance with LPSs from the south (Bourdier, 1958; Bonifay, 1965; Bosq et al., 2020b). Especially the reworking of the Eemian soil material as observed in the Baix LPS, followed by another phase of in situ pedogenesis, forming the 7 Btg horizon, agrees well with the deposits at the top of the S1 unit identified at the Collias LPS, ca. 100 km further south (Bwk developed in a reworked soil sediment with an OSL age of ca. 83 ka) and with similar horizons reported from LPSs in the Durance Valley (Fig. 1) (Bonifay, 1965; Bosq et al., 2020b).

Other local archives near the Baix LPS and in the Rhône Rift Valley also reflect our derived Eemian and early glacial climate conditions (Fig. 1). Eemian pollen records display summer-drought-resistant sclerophyllous taxa, with *Ilex*, *Olea*, *Pistacia* and evergreen *Quercus* (Beaulieu and Reille, 1984a; Tzedakis, 2007) and, at higher altitudes, mixed oak forest with the presence of *Buxus* and *Taxus* (Reille et al., 2000). The following change in vegetation towards tundra or steppe (Reille and Beaulieu, 1990; Mologni et al., 2021) was associated with a change to colder, drier, more continental climatic conditions, whereas the temperate deciduous vegetation recorded in between suggests a milder climate with higher precipitation and possibly higher temperatures. The gradual climate deterioration of the late Eemian is also reflected by the erosion of intensely weathered (partly red) sediments and a change within the pollen and human occupation remains derived from archaeological sites along the Ardèche and Payre rivers (Valladas et al., 2008; Rivals et al., 2009; Moncel et al., 2015) (Fig. 1).

4.2 Early glacial to Lower Pleniglacial transition

The erosional discontinuity above the7 Btg horizon reflects an unstable phase with slope-wash processes, during which material of the 7 Btg horizon was mixed with slope-wash loess, followed by a phase of loess accumulation. In a subsequent more stable phase, the lower interstadial palaeosol (represented by the 6 Bw3 horizon) developed. Loess accumulation again set in, while pedogenesis continued, as indicated by the gradual upper boundary of the lower interstadial palaeosol, which reflects the transition from predominating pedogenesis to predominating loess accumulation.

The OSL screening yielded "age estimates" of around 65–75 ka for the 6 BCk/Btg and 6 Bw3 horizons, suggesting the deposition took place during the transition from the late early glacial period (MIS 5a) to the Lower Pleniglacial (MIS 4). Thus, the erosion phase may correlate with Mélisey II (Guiter et al., 2003), whereas the subsequent more stable phase probably correlates with St Germain II (St Geneys 2 (Reille et al., 2000)) and/or Ognon I (Beaulieu and Reille, 1984b, 1989). The transition from the early glacial period to the Lower Pleniglacial in the Baix LPS is thus characterised by a marked climate deterioration. This agrees with central European LPSs, where unstable conditions are reflected by the Niedereschbach zone or Harmignies colluvial deposit (Antoine et al., 2016; Lehmkuhl et al., 2016). At the Collias LPS in the Rhône Rift Valley, this lower interstadial soil was

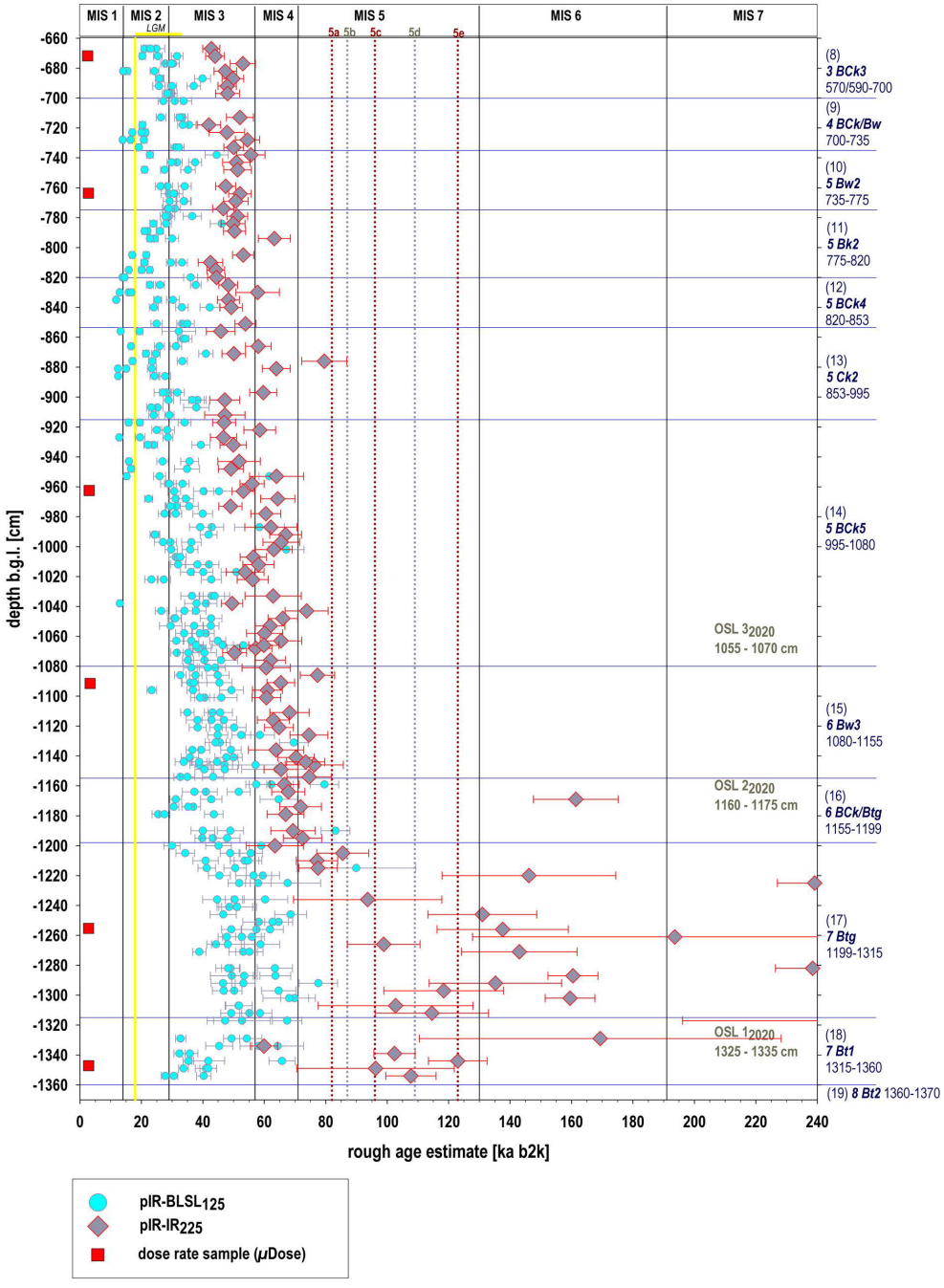

Figure 9. Results of the pIR-BLSL and $pIR_{60}IR_{225}$ screening of the Baix LPS, Rhône Rift Valley, SE France. Solid vertical lines denote the boundaries of marine isotope stages (MISs), while dotted lines denote the peaks of the MIS 5 substages. Boundaries after Lisiecki and Raymo (2005) and Railsback et al. (2015) (LGM denotes the Last Glacial Maximum).

not observed. However, intense slope-wash processes (Dmm horizon) during this period indicated unstable conditions at Collias as well (Bosq et al., 2020b). The pollen records of Les Échets and Velay (Beaulieu and Reille, 1984a, b) also indicate a shift to cooler and drier conditions, including a warmer phase within the general trend of climatic deterioration.

4.3 The Lower Pleniglacial

The following enhanced loess accumulation (highest silt content and U ratio) and decreasing weathering intensities (lowest clay content and clay / silt ratio) reflect drier and colder conditions (Fig. 11). The coarse silt fraction is interpreted as having been transported in short-term, near-surface to low suspension clouds within a relatively limited distance (Tsoar

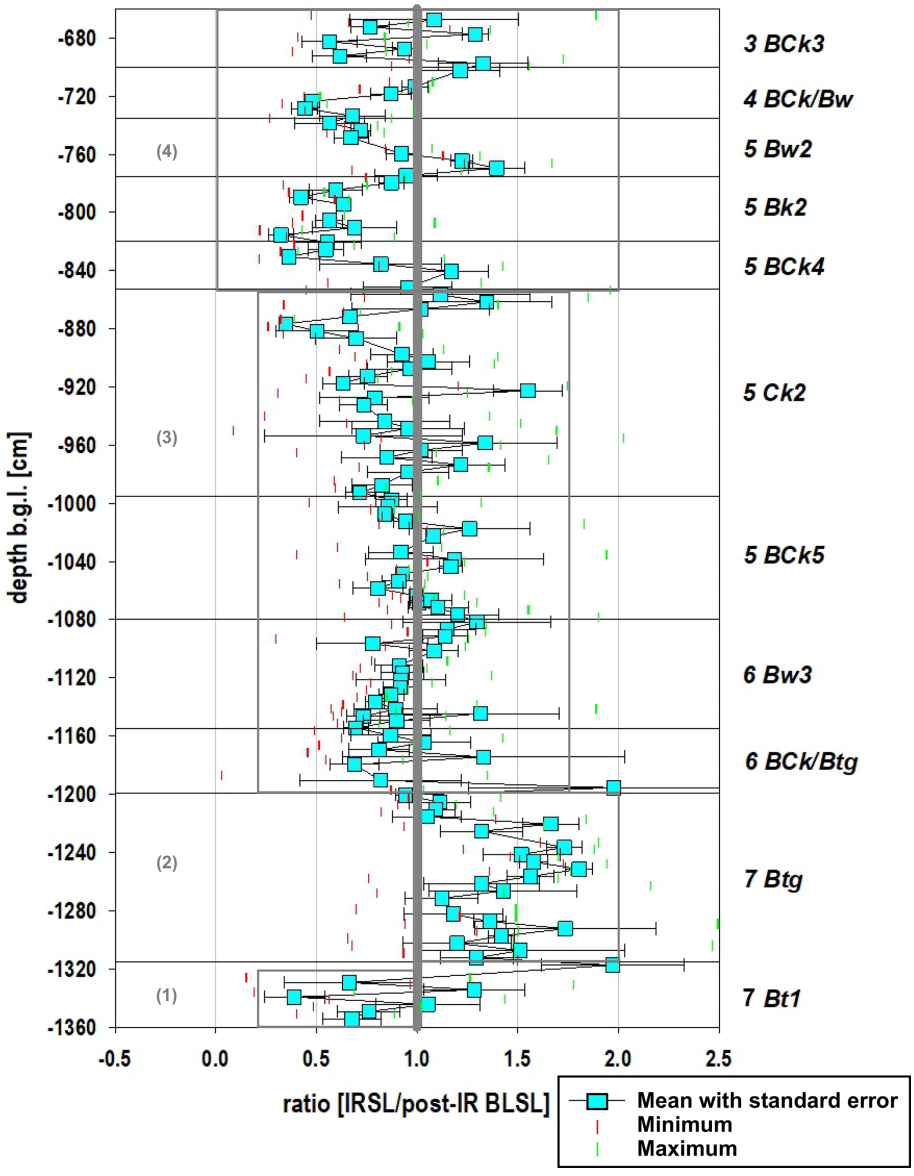

Figure 10. Results of the luminescence sensitivity measurements (IRSL/post-IR BLSL signal strength) of the Baix LPS, Rhône Rift Valley, SE France. Mean values with standard error of three aliquots measured per subsample with the pIR-BLSL protocol (blue squares and error bars in black) and respective minimum (red) and maximum (green) values (further details Sect. 2.3.2, "Luminescence screening"). Grey boxes mark subdivision into four units.

and Pye, 1987; Vandenberghe, 2013; Újvári et al., 2016). As it has been proven for other LPS sites along the Rhône Rift Valley (Bosq et al., 2018, 2020b), we also assume that the major part of the source of the loess deposits at the Baix LPS was the seasonally dried-out riverbed of the Rhône River during glacial times.

The only weakly weathered loess (5 BCk5 and 5 Ck2 horizons) reflects the predominance of loess accretion rates over soil formation rates during the Lower Pleniglacial at Baix, indicating generally dry and cold conditions. Also, the observed diverse forms and sizes of secondary carbonate accumulation (i.e. pseudomycelia, hard and soft carbonate nodules) and the upwardly increasing $CaCO_3$ contents suggest a weakening of carbonate leaching under increasingly drier conditions (Fig. 11).

This phase of enhanced loess deposition coincides with increased loess accumulation in most of the European, including Mediterranean, LPSs (Antoine et al., 2001; Ferraro, 2009; Zerboni et al., 2015) and with high sedimentation rates at other sites in the Rhône Rift Valley (Tricart, 1952; Sierro et al., 2009; Bosq et al., 2020b). The associated cold and dry climate is also reflected in the decline of trees to semi-open

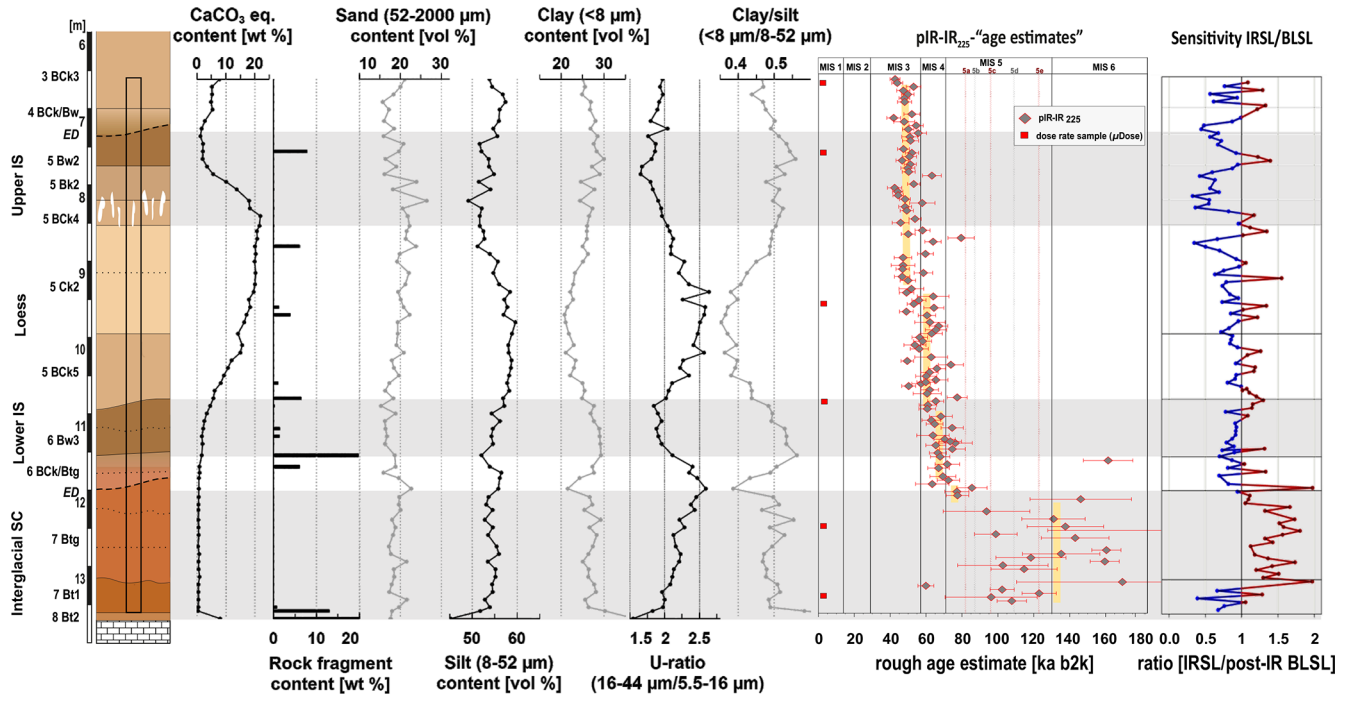

Figure 11. Synopsis of data for the lower 7 m of the Baix LPS, Rhône Rift Valley, SE France. From left to right: profile sketch (grey bars mark phases of soil formation); carbonate content (as $CaCO_3$ equivalent); rock-fragment content; contents of sand, silt and clay in the fine earth; U ratio; clay / silt ratio; "age estimates" based on the $pIR_{60}IR_{225}$ screening (solid lines denote the boundaries of marine isotope stages (MISs), dotted lines denote the peaks of the MIS 5 substages) and luminescence sensitivity (IRSL/pIR-BLSL) based on the $pIR_{125}BLSL_{125}$ protocol (SC, palaeosol complex; IS, interstadial palaeosol; ED, erosional discontinuity).

boreal landscape with partly steppe vegetation in the valley (Beaulieu and Reille, 1989; Reille et al., 2000; Moncel et al., 2015).

4.4 The Middle Pleniglacial

The upper interstadial palaeosol in the Baix LPS is interpreted to represent a strongly truncated and partially reworked Calcic Cambisol, including the reworked 5 Bw2 horizon, underlain by the in situ 5 Bk2 and 5 BCk4 horizons. Its basal large carbonate nodules require a corresponding carbonate source, i.e. a thick decarbonated soil horizon above. Therefore, we assume that the most intensively weathered upper part of the Calcic Cambisol was eroded. A phase of increased loess accumulation followed. The deposits in which the horizons 5 Ck2, 5 BCk4, 5 Bk2, 5 Bw2, 4 BCk/Bw and 3 BCk3 developed accumulated during the end of MIS 4 and into MIS 3 (Figs. 9, 11). The uppermost subsamples analysed from the 3 BCk3 horizon may point to slightly younger "age estimates" (~ 40 ka), as would be expected for sediment deposits above an in situ palaeosol. Fine-tuned alterations of screening "age estimates" may be camouflaged by possible subsample-to-subsample variations in radionuclide concentrations and water contents, which both have an impact on effective dose rates and OSL "age estimates" but were not considered for the simplified approach of the OSL screening. Nevertheless, the OSL screening supports the hypothesis that the strongly truncated upper interstadial Calcic Cambisol represents Middle Pleniglacial palaeosol remains. The soil formation phase might correspond to the interstadial periods of Pile–Goulotte (Moershoofd) dated to 50–43 ka and/or Charbon (Hengelo) (38–37 ka) (Guiot et al., 1993; Guiter et al., 2003). The assumed soil formation intensity of the Calcic Cambisol remains, including the prominent carbonate nodules, suggests temperate conditions with at least one phase of intense carbonate dissolution and reprecipitation. Comparably intensely developed brown truncated soil horizons are found in most of the European and Mediterranean LPSs, e.g. Remagen soils, Gräselberg soils (Antoine et al., 2001; Schirmer, 2016; Fischer et al., 2021; Wacha et al., 2011). In the Collias LPS in SE France, a very similar brown Bwk horizon with similar prominent carbonate nodules was identified. The likely period of this soil formation was after ~ 55 ka and had ended by ~ 39 ka, as suggested by OSL dating (Bosq et al., 2020b). During our field surveys, we observed the prominent carbonate nodules not only at Baix and Collias but also in several other LPSs in the Rhône Rift Valley. Therefore, these large cone-shaped carbonate nodules that underlie truncated remains of a brown Calcic Cambisol may serve as a useful stratigraphic marker in LPSs along the Rhône Rift Valley. Another possibly comparable brown soil horizon, al-

though without any age provided, was described for the LPS of the Durance Valley (Bonifay, 1965).

The local assumed temperate conditions are supported by the pollen of the MIS 3 interstadials, pointing to deciduous *Quercus* (at least from 39.405 ± 2250 BP), associated with *Abies* and *Carpinus* (Beaudouin et al., 2005). Thus, around $\sim 40\,000$ BP, the vegetation in the wider region was mainly composed of broad-leaved temperate taxa, whereas at higher altitudes, the last regional presence of *Picea* was recorded (Reille and Beaulieu, 1990; Beaudouin et al., 2005). With respect to the local hydrology, malacological analyses of a palustrine level at the site of Mignet College in Aix-en-Provence, correlating also with the Pile–Goulotte (Moershoofd) interstadial, pointed to a marsh habitat, which may support assumed enhanced humidity in the region for this period (Magnin and Bonnet, 2014).

5 Conclusion

Our investigations of the lower ca. 7 m of the Baix LPS in the Rhône Rift Valley confirm the importance of this archive for reconstructing regional Eemian to Middle Pleniglacial palaeoenvironmental changes. The obtained palaeoenvironmental reconstruction can be well correlated with other regional archives and can point out the different conditions compared to the central European LPSs. From bottom to top of the investigated part, we identified Eemian (MIS 5e) to early glacial (MIS 5d-a) soil formation, resulting in a polygenetic reddish Stagnic Luvisol; an early glacial (MIS 5a/4) to Lower Pleniglacial (MIS 4) brown horizon of a weakly developed Cambisol; a Lower to Middle Pleniglacial (MIS 4 to MIS 3) loess package showing subordinate synsedimentary pedogenesis; and, most prominently, a strongly truncated Middle Pleniglacial (MIS 3) Calcic Cambisol, underlain by characteristic large cone-shaped carbonate nodules. Thus, we can conclude that the generally characteristics of Baix in terms of the main soil formation and loess depositions phases coincide with central European LPSs, although their characteristics induced by climatic differences seem to reflect the transitional position of the LPSs.

However, we observed multiple reworkings and bioturbation, which are typical of the loess–palaeosol landscape of the Rhône Rift Valley and challenge numerical dating (Tricart, 1952; Bonifay 1965; Franc et al., 2017; Bosq et al., 2018, 2020b). We performed an optically stimulated luminescence (OSL) screening by applying a pIR_{60}-$BLSL_{125}$ and a pIR_{60}-IR_{225} single-aliquot regeneration (SAR) protocol to minimally prepared polymineral coarse grains on 126 ca. 1 cm^3 subsamples collected at vertical intervals of ca. 5 cm. Whereas the pIR-BLSL approach gave erroneously young "age estimates", the pIR-IR technique seems to provide a realistic time corridor ranging from bottom to top from MIS 5 into MIS 3, thus corroborating the field hypotheses of the likely temporal positions of the different loess and palaeosol horizons. We also monitored OSL sensitivity changes in the minimally prepared coarse grains along the investigated part of the profile wall and found patterns which appear plausible when related to the likely evolution of the terrestrial archive, i.e. with respect to weathering and pedogenesis as well as material input by aeolian and/or slopewash processes. Finally, among the known LPSs along the Rhône Rift Valley, the Baix LPS provides the most detailed, dated palaeoenvironmental record of the Eemian to Middle Pleniglacial landscape evolution. These promising results encourage continuation of the palaeoenvironmental analysis of the Baix LPS.

Data availability. All data are provided in the figures and table, and they are available upon request.

Supplement. The supplement related to this article is available online at: https://doi.org/10.5194/egqsj-73-1-2024-supplement.

Author contributions. Conceptualisation of the project: DS, AK; field investigation: NP, DS, AK; methodology: NP, AK, VK, TK, SK; data validation and interpretation: NP, DS, AK, VK, SK; conceptualisation of the manuscript: NP; writing – original draft preparation: NP; writing – review and editing: all authors.

All authors have read and agreed to the published version of the paper.

Competing interests. At least one of the (co-)authors is a member of the editorial board of *E&G Quaternary Science Journal*. The peer-review process was guided by an independent editor, and the authors also have no other competing interests to declare.

Disclaimer. Publisher's note: Copernicus Publications remains neutral with regard to jurisdictional claims made in the text, published maps, institutional affiliations, or any other geographical representation in this paper. While Copernicus Publications makes every effort to include appropriate place names, the final responsibility lies with the authors.

Acknowledgements. We are very grateful to Louis Garnier for allowing us to prepare and investigate the Baix LPS in his loam pit. We thank Barbara von der Lühe and Tianhao Wang for their help in the field and Marius Friedrich and Jutta Asmuth for the laboratory analyses. We also thank the European Union's Horizon 2020 research and innovation programme under the Marie Skłodowska-Curie grant agreement no. 844457 (CREDit), who supported Sebastian Kreutzer during the writing phase of this paper. We thank the two anonymous reviewers for their very constructive comments and suggestions, supporting the improvement and finalisation of the manuscript.

Financial support. This open-access publication was funded by the University of Göttingen.

Review statement. This paper was edited by Jan-Hendrik May and reviewed by two anonymous referees.

References

Aitken, M.J.: An introduction to optical dating: the dating of Quaternary sediments by the use of photon-stimulated luminescence, Oxford University Press, Oxford, UK, 280 pp., ISBN 0198540922, 1998.

Antoine, P., Rousseau, D., Zöller, L., Lang, A., Munaut, A.-V., Hatté, C., and Fontugne, M.: High-resolution record of the last Interglacial–glacial cycle in the Nussloch loess–palaeosol sequences, Upper Rhine Area, Germany, Quatern. Int., 76-77, 211–229. https://doi.org/10.1016/S1040-6182(00)00104-X, 2001.

Antoine, P., Rousseau, D.-D., Moine, O., Kunesch, S., Hatté, C., Lang, A., Tissoux, H., and Zöller, L.: Rapid and cyclic aeolian deposition during the Last Glacial in European loess: a high-resolution record from Nussloch, Germany, Quaternary Sci. Rev., 28, 2955–2973, https://doi.org/10.1016/j.quascirev.2009.08.001, 2009.

Antoine, P., Coutard, S., Guerin, G., Deschodt, L., Goval, E., Locht, J.-L., and Paris, C.: Upper Pleistocene loess-palaeosol records from Northern France in the European context: Environmental background and dating of the Middle Palaeolithic, Quatern. Int., 411, 4–24, https://doi.org/10.1016/j.quaint.2015.11.036, 2016.

Antoine, P., Coutard, S., Bahain, J.-J., Locht, J.-L., Hérisson, D., and Goval, E.: The last 750 ka in loess–palaeosol sequences from northern France: environmental background and dating of the western European Palaeolithic, J. Quaternary Sci., 36, 1293–1310, https://doi.org/10.1002/jqs.3281, 2021.

Bateman, M. D., Stein, S., Ashurst, R. A., and Selby, K.: Instant luminescence chronologies? High resolution luminescence profiles using a portable luminescence reader, Quat. Geochronol., 30, 141–146, https://doi.org/10.1016/j.quageo.2014.12.007, 2015.

Beaudouin, C., Suc, J.-P., Acherki, N., Courtois, L., Rabineau, M., Aloïsi, J.-C., Sierro, F. J., and Oberlin, C.: Palynology of the northwestern Mediterranean shelf (Gulf of Lions): First vegetational record for the last climatic cycle, Mar. Petrol. Geol., 22, 845–863, https://doi.org/10.1016/j.marpetgeo.2005.03.005, 2005.

Beuselinck, L., Govers, G., Poesen, J., Degraer, G., and Froyen, L.: Grain-size analysis by laser diffractometry: comparison with the sieve-pipette method, Catena, 32, 193–208, https://doi.org/10.1016/S0341-8162(98)00051-4, 1998.

Bibus, E. and Semmel, A.: Stratigraphische Leithorizonte im Würmlöß des Mittelrhein-Gebietes, Geol. Jb. Hessen, 105, 141–147, 1977.

Blume, H.-P., Stahr, K., and Leinweber, P.: Bodenkundliches Praktikum: Eine Einführung in pedologisches Arbeiten für Ökologen, insbesondere Land- und Forstwirte und für Geowissenschaftler, Spektrum Akademischer Verlag Heidelberg, 255 pp., ISBN 9783827415530, 2011.

Boixadera, J., Poch, R. M., Lowick, S. E., and Balasch, J. C.: Loess and soils in the eastern Ebro Basin, Quatern. Int., 376, 114–133, https://doi.org/10.1016/j.quaint.2014.07.046, 2015.

Bonifay, E.: Stratigraphie des loess anciens et récents dans le Sud-Est de la France, Quaternaire, 2, 21–34, 1965.

Bosq, M., Bertran, P., Degeai, J.-P., Kreutzer, S., Queffelec, A., Moine, O., and Morin, E.: Last Glacial aeolian landforms and deposits in the Rhône Rift Valley (SE France): Spatial distribution and grain-size characterization, Geomorphology, 318, 250–269, https://doi.org/10.1016/j.geomorph.2018.06.010, 2018.

Bosq, M., Bertran, P., Degeai, J.-P., Queffelec, A., and Moine, O.: Geochemical signature of sources, recycling and weathering in the Last Glacial loess from the Rhône Rift Valley (southeast France) and comparison with other European regions, Aeolian Res., 42, 100561, https://doi.org/10.1016/j.aeolia.2019.100561, 2020a.

Bosq, M., Kreutzer, S., Bertran, P., Degeai, J.-P., Dugas, P., Kadereit, A., Lanos, P., Moine, O., Pfaffner, N., Queffelec, A., and Sauer, D.: Chronostratigraphy of two late Pleistocene loess-palaeosol sequences in the Rhône Rift Valley (southeast France), Quaternary Sci. Rev., 106473, https://doi.org/10.1016/j.quascirev.2020.106473, 2020b.

Bourdier, F.: Le Bassin du Rhône au Quaternaire, géologie et préhistoire, PhD thesis, Faculté des Sciences de l'Université de Paris, 337 pp., https://theses.hal.science/tel-00682737 (last access: 17 December 2023), 1958.

Burbidge, C. I., Sanderson, D. C. W., Housley, R. A., and Allsworth Jones, P.: Survey of Palaeolithic sites by luminescence profiling, a case study from Eastern Europe, Quat. Geochronol., 2, 296–302, https://doi.org/10.1016/j.quageo.2006.05.024, 2007.

Chenevoy, M., Elmi, S., Lorenchet de Montjamont, M., Combier, J., and Michel, R.: Notice Explicative de la Feuille Crest à 1/50 000, Bureau de recherches géologiques et minières (BRGM), http://ficheinfoterre.brgm.fr/Notices/0842N.pdf (last access: 17 December 2023), 1977.

Costantini, E. A., Carnicelli, S., Sauer, D., Priori, S., Andreetta, A., Kadereit, A., and Lorenzetti, R.: Loess in Italy: Genesis, characteristics and occurrence, Catena, 168, 14–33, https://doi.org/10.1016/j.catena.2018.02.002, 2018.

Beaulieu, J.-L. and Reille, M.: A long Upper Pleistocene pollen record from Les Échets near Lyon, France, Boreas, 111–132, https://doi.org/10.1111/j.1502-3885.1984.tb00066.x, 1984a.

Beaulieu, J.-L. and Reille, M.: The Pollen Sequence of Les Échets (France): A New Element for the Chronology of the Upper Pleistocene, Geogr. Phys. Quatern., 38, 3–9, https://doi.org/10.7202/032531ar, 1984b.

Beaulieu, J.-L. and Reille, M.: The transition from temperate phases to stadials in the long upper Pleistocene sequence from Les Échets (France), Palaeogeogr. Palaeoecl., 72, 147–159, https://doi.org/10.1016/0031-0182(89)90139-9, 1989.

Beaulieu, J.-L. and Reille, M.: The last cycle at La Grande Oile (Vosges, France), Quaternary Sci. Rev., 11, 431–438, https://doi.org/10.1016/0277-3791(92)90025-4, 1992.

FAO: Guidelines for soil description. Food and Agriculture Organization of the United Nations, Rome, Italy, ISBN 92-5-105521-1, 2006.

Ferraro, F.: Age, sedimentation, and soil formation in the Val Sorda loess sequence, Northern Italy, Quatern. Int., 204, 54–64, https://doi.org/10.1016/j.quaint.2008.12.002, 2009.

Fischer, P., Jöris, O., Fitzsimmons, K. E., Vinnepand, M., Prud'homme, C., Schulte, P., Hatté, C., Hambach, U., Lindauer, S., Zeeden, C., Peric, Z., Lehmkuhl, F., Wunderlich, T., Wilken, D., Schirmer, W., and Vött, A.: Millennial-scale terrestrial ecosystem responses to Upper Pleistocene climatic changes: 4D-reconstruction of the Schwalbenberg Loess-Palaeosol-Sequence (Middle Rhine Valley, Germany), Catena, 196, 104913, https://doi.org/10.1016/j.catena.2020.104913, 2021.

Fitzsimmons, K. E., Perić, Z., Nowatzki, M., Lindauer, S., Vinnepand, M., Prud'homme, C., Dave, A. K., Vött, A., and Fischer, P.: Luminescence Sensitivity of Rhine Valley Loess: Indicators of Source Variability?, Quaternary, 5, 1, https://doi.org/10.3390/quat5010001, 2022.

Franc, O., Moine, O., Fülling, A., Auguste, P., Pasty, J.-F., Gadiolet, P., Gaertner, V., and Robert, V.: Les séquences alluvio-lœssiques du Würm moyen/supérieur de Quincieux et de Lyon (Rhône-Alpes, France): premières interprétations paléoenvironnementales et corrélations, Quaternaire, 28, 423–453, https://journals.openedition.org/quaternaire/8453 (last access: 17 December 2023), 2017.

Galbraith, R. F., Roberts, R. G., Laslett, G. M., Yoshida, H., and Olley, J. M.: Optical dating of single grains of quartz from Jinmium rock shelter, northern Australia. Part I: experimental design and statistical models, Archaeometry, 41, 339–364, https://doi.org/10.1111/j.1475-4754.1999.tb00987.x, 1999.

Godfrey-Smith, D. I., Huntley, D. J., and Chen, W.-H.: Optical dating studies of quartz and feldspar sediment extracts, Quaternary Sci. Rev., 373–380, https://doi.org/10.1016/0277-3791(88)90032-7, 1988.

Guenard, V., Drobinski, P., Caccia, J.-L., Campistron, B., and Benech, B.: An observational study of the mesoscale Mistral dynamics, Bound.-Lay. Meterol., 115, 263–288, https://doi.org/10.1007/s10546-004-3406-z, 2005.

Guenther, E. W.: Zur Gliederung der Lösse des südlichen Oberrheintals, E&G Quaternary Sci. J., 37, 67–78, https://doi.org/10.3285/eg.37.1.07, 1987.

Günster, N., Eck, P., Skowronek, A., and Zöller, L.: Late Pleistocene loess and their paleosols in the Granada Basin, Southern Spain, Quatern. Int., 76–77, 241–245, https://doi.org/10.1016/S1040-6182(00)00106-3, 2001.

Guérin, G., Mercier, N., and Adamiec, G.: Dose-rate conversion factors: update, Ancient TL, 29, 5–8, https://www.aber.ac.uk/en/media/departmental/dges/ancienttl/pdf/vol29no1/atl-issue29-1.pdf#page=9 (last access: 15 November 2022), 2011.

Guiot, J., Beaulieu, J. L., Cheddadi, R., David, F., Ponel, P., and Reille, M.: The climate in Western Europe during the last Glacial/Interglacial cycle derived from pollen and insect remains, Palaeogeogr. Palaeoecl., 103, 73–93, https://doi.org/10.1016/0031-0182(93)90053-L, 1993.

Guiter, F., Andrieu-Ponel, V., Beaulieu, J.-L., Cheddadi, R., Calvez, M., Ponel, P., Reille, M., Keller, T., and Goeury, C.: The last climatic cycles in Western Europe: a comparison between long continuous lacustrine sequences from France and other terrestrial records, Quatern. Int., 111, 59–74, https://doi.org/10.1016/S1040-6182(03)00015-6, 2003.

Haesaerts, P., Damblon, F., Gerasimenko, N., Spagna, P., and Pirson, S.: The Late Pleistocene loess-palaeosol sequence of Middle Belgium, Quatern. Int., 411, 25–43, https://doi.org/10.1016/j.quaint.2016.02.012, 2016.

IGN-FR: l'Institut national de l'information géographique et forestière, https://geoservices.ign.fr, last access: 24 May 2020.

ISO 11277: Soil quality - Determination of particle size distribution in mineral soil - Method by sieving and sedimentation, ISO, 2020.

ISO 13320: Particle size analysis – Laser diffraction methods, ISO, 2020.

IUSS Working Group WRB: World Reference Base for Soil Resources, International soil classification system for naming soils and creating legends for soil maps, 4th edn., International Union of Soil Sciences (IUSS), Vienna, Austria, ISBN: 979-8-9862451-1-9, 2022.

Joly, D., Brossard, T., Cardot, H., Cavailhes, J., Hilal, M., and Wavresky, P.: Ley types de climats en France, une construction spatiale. Cybergeo, Eur. J. Geogr., Cartographie, Imagerie, SIG, document 501, https://doi.org/10.4000/cybergeo.23155, 2010.

Kadereit, A., Kreutzer, S., Schmidt, C., and DeWitt, R.: Author Comment 1, AC1: 'A closer look at IRSL SAR fading data and their implication for luminescence dating, https://doi.org/10.5194/gchron-2020-3-AC1, 2020.

Kinnaird, T. C., Sanderson, D. C. W., and Woodward, N. L.: Applying luminescence methods to geoarchaeology: a case study from Stronsay, Orkney, Earth Env. Sci. T. R. So., 102, 191–199, https://doi.org/10.1017/S1755691012011115, 2012.

Kolb, T., Tudyka, K., Kadereit, A., Lomax, J., Poręba, G., Zander, A., Zipf, L., and Fuchs, M.: The μDose system: determination of environmental dose rates by combined alpha and beta counting – performance tests and practical experiences, Geochronology, 4, 1–31, https://doi.org/10.5194/gchron-4-1-2022, 2022.

Konert, M. and Vandenberghe, J.: Comparison of laser grain size analysis with pipette and sieve analysis: a solution for the underestimation of the clay fraction, Sedimentology, 44, 523–535, https://doi.org/10.1046/j.1365-3091.1997.d01-38.x, 1997.

Kreutzer, S., Schmidt, C., Fuchs, M. C., Dietze, M., Fischer, M., and Fuchs, M.: Introducing an R package for luminescence dating analysis, Ancient TL, 30, 1–8, hdl:10013/epic.44194.d001, 2012.

Kreutzer, S., Schmidt, C., DeWitt, R., and Fuchs, M.: The a-value of polymineral fine grain samples measured with the post-IR IRSL protocol, Radiat. Meas., 69, 18–29, https://doi.org/10.1016/j.radmeas.2014.04.027, 2014.

Kreutzer, S., Valladas, H., Texier, P.-J., Moineau, V., Mologni, C., and Mercier, N.: The Mousterian loess sequence La Combette (France) and its chronological framework: A re-investigation, C. R. Palevol., 225–525, https://doi.org/10.5852/cr-palevol2021v20a14, 2021.

Lai, Z., Zöller, L., Fuchs, M., and Brückner, H.: Alpha efficiency determination for OSL of quartz extracted from Chinese loess, Radiat. Meas., 43, 767–770, https://doi.org/10.1016/j.radmeas.2008.01.022, 2008.

Lapp, T., Jain, M., Thomsen, K. J., Murray, A. S., and Buylaert, J.-P.: New luminescence measurement facilities in retrospective dosimetry, Radiat. Meas., 47, 803–808, https://doi.org/10.1016/j.radmeas.2012.02.006, 2012.

Lapp, T., Kook, M., Murray, A. S., Thomsen, K. J., Buylaert, J.-P., and Jain, M.: A new luminescence detection and stimulation head for the Risø TL/OSL reader, Radiat. Meas., 81, 178–184, https://doi.org/10.1016/j.radmeas.2015.02.001, 2015.

Lehmkuhl, F., Zens, J., Krauß, L., Schulte, P., and Kels, H.: Loess-paleosol sequences at the northern European loess belt in Germany: Distribution, geomorphology and stratigraphy, Quaternary Sci. Rev., 153, 11–30, https://doi.org/10.1016/j.quascirev.2016.10.008, 2016.

Lehmkuhl, F., Nett, J. J., Pötter, S., Schulte, P., Sprafke, T., Jary, Z., Antoine, P., Wacha, L., Wolf, D., Zerboni, A., Hosek., J., Markovic, S. B., Obreth, I., Sümegi, P., Veres, D., Zeeden, C., Boemke, B., Viehweger, J., and Hambach, U.: Loess landscapes of Europe–Mapping, geomorphology and zonal differentiation, Earth-Sci. Rev., 215, 103496, https://doi.org/10.1016/j.earscirev.2020.103496, 2021.

Lisiecki, L. E. and Raymo, M. E.: A Pliocene-Pleistocene stack of 57 globally distributed benthic δ^{18}O records, Paleoceanography, 20, PA1003, https://doi.org/10.1029/2004PA001071, 2005.

Magnin, F. and Bonnet, S.: Une succession malacologique du pléniglaciaire moyen et du postglaciaire à Aix-en-Provence (France) éléments de datation, taphonomie des assemblages et paléoenvironnements, Quaternaire, 163–185, https://doi.org/10.4000/quaternaire.7040, 2014.

Marković, S. B., Hambach, U., Catto, N., Jovanović, M., Buggle, B., Machalett, B., Zöller, L., Glaser, B., and Frechen, M.: Middle and Late Pleistocene loess sequences at Batajnica, Vojvodina, Serbia, Quatern. Int., 198, 255–266, https://doi.org/10.1016/j.quaint.2008.12.004, 2009.

May, J.-H., Marx, S. K., Reynolds, W., Clark-Balzana, L., Jacobsen, G. E., and Preusser, F.: Establishing a chronological framework for a late Quaternary seasonal swamp in the Australian 'Top End', Quat. Geochronol., 47, 81–92, https://doi.org/10.1016/j.quageo.2018.05.010, 2018.

Mazenot, G.: Recherches sur les faunes malacologiques du loess récent würmien et de divers limons terrestres holocènes dans le sud-est de la France (pp. 1–16), Publications de la Société Linnéenne de Lyon, 25, 9–24, https://doi.org/10.3406/linly.1956.7784, 1956.

Meteo-France: Fiche Climatologique, Statistiques 1991–2020 et records Valence-Chabeui, https://donneespubliques.meteofrance.fr/?fond=produit&id_produit=117&id_rubrique=39 (last access: 17 December 2023), 2021.

Moine, O., Rousseau, D.-D., and Antoine, P.: Terrestrial molluscan records of Weichselian Lower to Middle Pleniglacial climatic changes from the Nussloch loess series (Rhine Valley, Germany): the impact of local factors, Boreas, 34, 363–380, https://doi.org/10.1111/j.1502-3885.2005.tb01107.x, 2005.

Mologni, C., Purdue, L., Audiard, B., Dubar, M., Kreutzer, S., and Texier, P.-J.: Sedimentary processes and palaeoenvironments from La Combette sequence (southeastern France): climatic insights on the Last Interglacial/Glacial transition, Palaeogeogr. Palaeoecl., 576, 110503, https://doi.org/10.1016/j.palaeo.2021.110503, 2021.

Moncel, M.-H., Allué, E., Bailon, S., Barshay-Szmidt, C., Béarez, P., Crégut, É., Daujeard, C., Desclaux, E., Debard, É., Lartigot-Campin, A.-S., Puaud, S., and Roger, T.: Evaluating the integrity of palaeoenvironmental and archaeological records in MIS 5 to 3 karst sequences from southeastern France, Quatern. Int., 378, 22–39, https://doi.org/10.1016/j.quaint.2013.12.009, 2015.

Muñoz-Salinas, E., Bishop, P., Sanderson, D. C. W., and Zamorano, J.-J.: Interpreting luminescence data from a portable OSL reader: three case studies in fluvial settings, Earth Surf. Proc. Land., 36, 651–660, https://doi.org/10.1002/esp.2084, 2011.

Muñoz-Salinas, E., Bishop, P., Sanderson, D., and Kinnaird, T.: Using OSL to assess hypotheses related to the impacts of land use change with the early nineteenth century arrival of Europeans in south-eastern Australia: an exploratory case study from Grabben Gullen Creek, New South Wales, Earth Surf. Proc. Land., 39, 1576–1586, https://doi.org/10.1002/esp.3542, 2014.

Murray, A. S. and Wintle, A. G.: Luminescence dating of quartz using an improved single-aliquot regenerative-dose protocol, Radiat. Meas., 32, 57–73, https://doi.org/10.1016/S1350-4487(99)00253-X, 2000.

Pastre, J.-F., Singer, B. S., Guillou, H., Pupin, J.-P., and Riou, B.: Chronostratigraphy of the key Upper Miocene (Lower Turolian) sequence of la Montagne d'Andance (Ardèche, France). Implications of new 40Ar/39Ar laser fusion and unspiked K-Ar dating of trachytic tephra and basalts, B. Soc. Geol. Fr., 175, 3–10, https://doi.org/10.2113/175.1.3, 2004.

Portenga, E. W. and Bishop, P.: Confirming geo-morphological interpretations based on portable OSL reader data, Earth Surf. Proc. Land., 41, 427–432, https://doi.org/10.1002/esp.3834, 2016.

Railsback, B., Gibbard, P. L., Head, M. J., Voarintsoa, N. R. G., and Toucanne, S.: An optimized scheme of lettered marine isotope substages for the last 1.0 million years, and the climatostratigraphic nature of isotope stages and substages, Quaternary Sci. Rev. 111, 94–106, https://doi.org/10.1016/j.quascirev.2015.01.012, 2015.

Reille, M. and de Beaulieu, J. L.: Pollen analysis of a long upper Pleistocene continental sequence in a Velay maar (Massif Central, France), Palaeogeogr. Palaeoecl., 80, 35–48, https://doi.org/10.1016/0031-0182(90)90032-3, 1990.

Reille, M., Beaulieu, J.-L., Svobodova, H., Andrieu-Ponel, V., and Goeury, C.: Pollen analytical bio-stratigraphy of the last five climatic cycles from a long continental sequence from the Velay region (Massif Central, France), J. Quaternary Sci., 15, 665–685, https://doi.org/10.1002/1099-1417(200010)15:7<665::AID-JQS560>3.0.CO;2-G, 2000.

Rivals, F., Moncel, M.-H., and Patou-Mathis, M.: Seasonality and intra-site variation of Neanderthal occupations in the Middle Palaeolithic locality of Payre (Ardèche, France) using dental wear analyses, J. Archaeol. Sci., 36, 1070–1078, https://doi.org/10.1016/j.jas.2008.12.009, 2009.

Saint Martin, M.: Carte géologique harmonisée du département de l'Ardèche notice technique, BRGM, BRGM/RP-57097-FR, 423 pp., http://infoterre.brgm.fr/rapports/RP-57097-FR.pdf (last access: 11 February 2022), 2009.

Sanderson, D. C. W. and Murphy, S.: Using simple portable OSL measurements and laboratory characterisation to help understand complex and heterogeneous sediment sequences for luminescence dating, Quat. Geochronol., 5, 299–305, https://doi.org/10.1016/j.quageo.2009.02.001, 2010.

Sanderson, D. C. W., Bishop, P., Stark, M. T., and Spencer, J. Q.: Luminescence dating of anthropogenically reset canal sediments from Angkor Borei, Mekong Delta, Cambodia, Quaternary Sci. Rev., 22, 1111–1121, https://doi.org/10.1016/S0277-3791(03)00055-6, 2003.

Sauer, D., Kadereit, A., Kühn, P., Kösel, M., Miller, C. E., Shinonaga, T., Kreutzer, S., Herrmann, L., Fleck, W., Starkovich, B.

M., and Stahr, K.: The loess-palaeosol sequence of Datthausen, SW Germany: Characteristics, chronology, and implications for the use of the Lohne Soil as a marker soil, Catena, 146, 10–29, https://doi.org/10.1016/j.catena.2016.06.024, 2016.

Schirmer, W.: Compendium of the Rhein loess sequence, At: Ikinger, A. and Schirmer, W. (Eds.): Loess units and solcomplexes in the Niederrhein and Maas area, Terra Nostra, 1, 102–104, 2002.

Schirmer, W.: Late Pleistocene loess of the Lower Rhine, Quatern. Int., 411, 44–61, https://doi.org/10.1016/j.quaint.2016.01.034, 2016.

Schulte, P. and Lehmkuhl, F.: The difference of two laser diffraction patterns as an indicator for post-depositional grain size reduction in loess-paleosol sequences, Palaeogeogr. Palaeoecl., 509, 126–136, https://doi.org/10.1016/j.palaeo.2017.02.022, 2018.

Schulte, P., Sprafke, T., Rodrigues, L., and Fitzsimmons, K. E.: Are fixed grain size ratios useful proxies for loess sedimentation dynamics? Experiences from Remizovka, Kazakhstan, Aeolian Res., 31, 131–140, https://doi.org/10.1016/j.aeolia.2017.09.002, 2018.

Sierro, F. J., Andersen, N., Bassetti, M. A., Berné, S. Canals, M., Curtis, J. H., Dennielou, B., Flores, J. A., Frigola, J., Gonzalez-Mora, B., Grimalt, J. O., Hodell, D. A., Jouet, G., Pérez-Folgado, M., and Schneider, R.: Phase relationship between sea level and abrupt climate change, Quaternary Sci. Rev., 28, 2867–2881, https://doi.org/10.1016/j.quascirev.2009.07.019, 2009.

Stoops, G.: Guidelines for Analysis and Description of Soil and Regolith Thin Sections, 2nd edn., ASA, CSSA, and SSSA Bks, American Society of Agronomy, Newark, 259 pp., ISBN: 978-0891189756, 2021.

Suen, T.-Y.: Le Loess de la Vallée du Rhône, Lyon : Bosc frères, M. et L. Riou, PhD Thèse, Université de Lyon-Faculté des Lettres, 163 pp., 1934.

Thiel, C., Buylaert, J.-P., Murray, A., Terhorst, B., Hofer, I., Tsukamoto, S., and Frechen, M.: Luminescence dating of the Stratzing loess profile (Austria) – Testing the potential of an elevated temperature post-IR IRSL protocol, Quatern. Int., 234, 23–31, https://doi.org/10.1016/j.quaint.2010.05.018, 2011.

Thomsen, K. J., Murray, A. S., Jain, M., and Bøtter-Jensen, L.: Laboratory fading rates of various luminescence signals from feldspar-rich sediment extracts, Radiat. Meas., 43, 1474–1486, https://doi.org/10.1016/j.radmeas.2008.06.002, 2008.

Tricart, J.: Paléoclimats quaternaires et morphologie climatique dans le Midi Méditerranéen, E&G Quaternary Sci. J., 2, 172–188, https://doi.org/10.3285/eg.02.1.20, 1952.

Tsoar, H. and Pye, K.: Dust transport and the question of desert loess formation, Sedimentology, 34, 139–153, https://doi.org/10.1111/j.1365-3091.1987.tb00566.x, 1987.

Tudyka, K., Miłosz, S., Adamiec, G., Bluszcz, A., Poręba, G., Paszkowski, Ł., and Kolarczyk, A.: μDose: A compact system for environmental radioactivity and dose rate measurement, Radiat. Meas., 118, 8–13, https://doi.org/10.1016/j.radmeas.2018.07.016, 2018.

Tudyka, K., Bluszcz, A., Poręba, G., Miłosz, S., Adamiec, G., Kolarczyk, A., Kolb, T., Lomax, J., and Fuchs, M.: Increased dose rate precision in combined α and β counting in the μDose system-a probabilistic approach to data analysis, Radiat. Meas., 134, 106310, https://doi.org/10.1016/j.radmeas.2020.106310, 2020.

Tzedakis, P. C.: Seven ambiguities in the Mediterranean palaeoenvironmental narrative, Quaternary Sci. Rev., 26, 2042–2066, https://doi.org/10.1016/j.quascirev.2007.03.014, 2007.

Újvári, G., Kok, J. F., Varga, G., and Kovács, J.: The physics of wind-blown loess: Implications for grain size proxy interpretations in Quaternary paleoclimate studies, Earth-Sci. Rev., 154, 247–278, https://doi.org/10.1016/j.earscirev.2016.01.006, 2016.

Valladas, H., Mercier, N., Ayliffe, L. K., Falguères, C., Bahain, J.-J., Dolo, J.-M., Froget, L., Joron, J.-L., Masaoudi, H., Reyss, J.-L., and Moncel, M.-H.: Radiometric dates for the Middle Palaeolithic sequence of Payre (Ardèche, France), Quat. Geochronol., 3, 377–389, https://doi.org/10.1016/j.quageo.2008.01.001, 2008.

Vandenberghe, J.: Grain size of fine-grained windblown sediment: A powerful proxy for process identification, Earth Sci. Rev., 121, 18–30, https://doi.org/10.1016/j.earscirev.2013.03.001, 2013.

Wacha, L., Mikulčić Pavlaković, S., Novothny, Á., Crnjaković, M., and Frechen, M.: Luminescence dating of Upper Pleistocene loess from the Island of Susak in Croatia, Quatern. Int., 234, 50–61, https://doi.org/10.1016/j.quaint.2009.12.017, 2011.

Woillard, G.: Grand Pile peat bog: a continuous pollen record for the last 140,000 years, Quaternary Res., 9, 1–21, https://doi.org/10.1016/0033-5894(78)90079-0, 1987.

Wolf, D., Ryborz, K., Kolb, T., Calvo Zapata, R., Sanchez Vizcaino, J., Zöller, L., and Faust, D.: Origins and genesis of loess deposits in central Spain, as indicated by heavy mineral compositions and grain-size variability, Sedimentology 62, 1139–1161, https://doi.org/10.1111/sed.12539, 2019.

Zech, M., Rass, S., Buggle, B., Löscher, M., and Zöller, L.: Reconstruction of the late Quaternary paleoenvironments of the Nussloch loess paleosol sequence, Germany, using n-alkane biomarkers, Quaternary Res., 78, 226–235, https://doi.org/10.1016/j.yqres.2012.05.006, 2012.

Zerboni, A., Trombino, L., Frigerio, C., Livio, F., Berlusconi, A., Michetti, A. M., Rodnight, H., and Spötl, C.: The loess-paleosol sequence at Monte Netto: a record of climate change in the Upper Pleistocene of the central Po Plain, northern Italy, J. Soil Sediments, 15, 1329–1350, https://doi.org/10.1007/s11368-014-0932-2, 2015.